Dynamic polymer hydrogels as synthetic extracellular matrices for 3D cell culture

Liu, T.

CHAPTER 2

Squaramide-based supramolecular materials drive HepG2 spheroid differentiation

2.1 Abstract

A major challenge in the use of HepG2 cell culture models for drug toxicity screening is their lack of maturity in 2D culture. 3D culture in Matrigel promotes the formation of spheroids that express liver-relevant markers, yet they still lack various primary hepatocyte functions. Therefore, alternative matrices where chemical composition and materials properties are controlled to steer maturation of HepG2 spheroids remain desired. Herein, a modular approach was taken based on a fully synthetic and minimalistic supramolecular matrix based on squaramide synthons outfitted with a cell-adhesive peptide, RGD for 3D HepG2 spheroid culture. Co-assemblies of RGD-functionalized squaramide-based and native monomers resulted in soft and self-recovering supramolecular hydrogels with a tunable RGD concentration. HepG2 spheroids were self-assembled and grown (~150 μm) within the supramolecular hydrogels with high cell viability and maturation over a 21-day culture. Importantly, significantly higher mRNA and protein expression levels of phase I and II metabolic enzymes, drug transporters and liver markers were found for the squaramide hydrogels in comparison to Matrigel. Overall, the fully synthetic squaramide hydrogels were proven to be synthetically accessible and effective for HepG2 differentiation showcasing the potential of this supramolecular matrix to rival and replace naturally-derived materials classically used in high-throughput toxicity screening.

2.2 Introduction

The liver is a critical organ of the human body that performs the biotransformation of drugs and other xenobiotics. Chemical transformations, such as oxidation, reduction, hydrolysis or other organic reactions, of these foreign agents give rise to active or inactive metabolites that can even be hepatotoxic.[1] Toxic insults to the liver from drug metabolites can eventually result in acute or chronic failure, otherwise known as drug-induced liver injury (DILI). DILI can occur from nearly every class of medication, and when encountered often results in abandonment of the therapy.[2] Thus, a major challenge in the drug discovery pipeline is to more accurately predict DILI early on, as hepatotoxic responses observed in animal models do not fully recapitulate those observed in humans resulting in drug candidates that fail in late stage clinical trials or even after approval in the clinic.[3]

Primary human hepatocytes (PHH) are the current gold standard for *in vitro* modeling of liver metabolism and toxicity as they represent 70% of total liver cell population. However, these cells are challenged by their limited availability and high donor variability, rapid loss of metabolic activity once harvested for *ex vivo* culture and costly derivation.[4,5] As an alternative cell source to model liver hepatic processes *in vitro*, human liver carcinoma cells (HepG2) are used due their wide availability, immortality, facile handling and stable phenotype in culture. However, these cells often show low expression levels of metabolic enzymes, namely cytochrome P450s that are relevant for xenobiotic metabolism, which has been correlated with the 2D culture methods used to expand them.[6] Three-dimensional (3D) culture methods have been used to improve the metabolic characteristics of HepG2 cells mainly using Matrigel, a biological matrix derived from murine tumor tissues, consisting of laminin, collagen IV, and entactin.[7] When encapsulated in Matrigel, HepG2 cells self-organize into

spheroidal structures and differentiate resulting in increased levels of various metabolic markers and can be dosed repeatedly with increased sensitivity to various hepatotoxic agents in comparison to HepG2 cells cultured in 2D.[8,9] However, Matrigel is costly, lacks definition with lot-to-lot variability,[7] its murine origin is problematic for some applications and chemical modification or decoupling of cues is difficult, leading to the exploration of synthetic polymers for use in 3D hepatocyte culture.

Matrices held together by covalent and non-covalent interactions have demonstrated the capacity to form spheroids from liver-derived cells in 3D, including a handful of recent reports examining the effect of cell interactive moieties to facilitate their differentiation and culture with varying degrees of success.[10–19] More recent studies have examined the capacity of the short integrin-binding peptide RGD to guide this process highlighting the importance of peptides derived from extracellular matrix proteins in synthetic materials. While a fully synthetic and covalent PEG hydrogel functionalized with RGD supported the growth of liver organoids, the addition of laminin-entactin complex was necessary for a non-covalent hydrogel based on a polyisocyanopeptide polymer to stimulate cell proliferative pathways demonstrating the importance of peptide concentration.[17,18] We thus became interested in examining a supramolecular polymer matrix based on stacked monomers for HepG2 cell culture to improve their growth and differentiation in 3D. However, such supramolecular systems that have the short peptides derived from matrix proteins is yet to be explored for the preparation of HepG2 spheroids, but can more broadly provide a powerful synthetic polymer platform for 3D cell culture where the peptide concentration can be tuned easily and facile cell seeding and release can be achieved.

In order to construct supramolecular polymer materials, monomers that contain highly directional, specific and reversible non-covalent interactions are needed.[20–24] In particular, squaramide synthons because of their ditopic presentation of hydrogen bond donors and acceptors on a minimal scaffold in combination with their synthetic

accessibilty are of interest for this aim.[25–32] We recently demonstrated their application in a tripodal hydrogelator for the culture of human induced pluripotent stem cells (hiPSCs), using the soft and self-recovering nature of the supramolecular matrix that supports cell self-assembly into spheroids driven by cell-cell contacts.[31] However, cell proliferation within these materials was found to be limited, pointing out the need to further modify this synthetic matrix with bioactive peptides to enable cell-matrix interaction. One short peptide that has been implemented in materials to provide such interactions is the RGD peptide, a short sequence derived from the FN-III repeat in the 10th domain of fibronectin, that binds the α5β1 and αVβ3 integrins on the cell surface. We therefore sought to introduce this cell-adhesive peptide within squaramide-based supramolecular materials through co-assembly of functional monomers as a facile means to tune peptide concentration for applications in 3D HepG2 culture and differentiation.
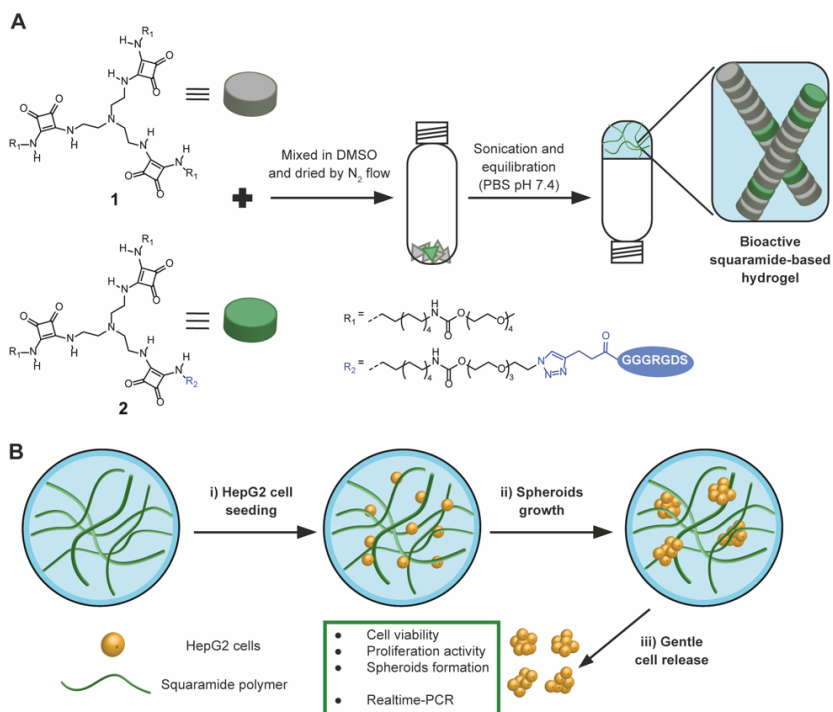
Scheme 2.1. A) Preparation of bioactive squaramide-based supramolecular hydrogels: RGD-functionalized squaramide monomers (**2**) were mixed with the native tripodal monomer (**1**) in DMSO. The dried solid was rehydrated in phosphate buffered saline (PBS, pH 7.4) by sonication, followed by being left to equilibrate overnight to obtain the co-assembled bioactive hydrogels. B) HepG2 spheroids cultured in bioactive squaramide-based supramolecular hydrogel for 21 days: i) HepG2 cells were mixed and encapsulated within the hydrogel by pipetting using its self-recovery property; ii) HepG2 cells self-assemble into spheroids, proliferate and differentiate within the hydrogel; iii) HepG2 spheroids were released by dilution and used for further analysis including cell proliferation and gene expression.

2.3 Results and Discussion

Design, synthesis and co-assembly of RGD-modified squaramide monomers to form bioactive supramolecular materials. Earlier, we designed a tripodal squaramide-based monomer (**1**) where three squaramides were embedded within a hydrophobic core consisting of tris(2-aminoethylamine) (TREN), aliphatic and a peripheral hydrophilic domain with oligo(ethylene glycol) chains. In this study, we further sought to incorporate the RGD peptide into these squaramide monomers (molecule **2**) to aid in cell proliferation, but also to provide a cell adhesive contact for cells (Scheme 2.1). However, the lack of reactive handle, namely the terminal methyl group on the oligo(ethylene glycol) chains of the monomer preclude it from further functionalization with any cargo, such as fluorescent dyes, crosslinkers, peptides or proteins. Therefore, a desymmetrized tripodal squaramide-based monomer where one of the three arms was end-functionalized with an azide (molecule **3**) was designed and synthesized starting from a monotrityl-protected TREN core. The azide functionality was first introduced onto tetraethylene glycol by tosylation (Scheme S2.1).[33] The tetraethylene glycol monomethyl ether and monoazide tetraethylene glycol were then independently activated using 1,1-carbonyldiimidazole and further reacted with monotrityl-protected C10 diamine in presence of N,N-Diisopropylethylamine (DIPEA) resulting in yields of 63% (methyl-terminated) and 74% (azide-terminated), respectively. The trityl protecting group was deprotected by TFA under an inert atmosphere, followed by its subsequent reaction with dibutyl squarate to provide the methyl-terminated and azide-terminated squaramide amphiphiles in yields of 87% and 47%, respectively (Scheme S2.2). Subsequently, the methyl-terminated squaramide amphiphile was reacted onto the desymmetrized TREN core resulting in a yield of 54%. Lastly, the trityl group on TREN core was deprotected using TFA and further coupled to the azide-terminated squaramide amphiphile giving the final compound **3** in a 56% yield (Scheme S2.3). The

RGD peptides (GGGRGDS, **PEP1**) were then synthesized by solid-phase peptide synthesis with the introduction of 4-pentyonic acid at the N-terminus to provide a reactive handle for bioconjugation. In a final step, the alkyne-ended RGD peptides (**PEP2**) were coupled to molecule **3** by copper(I)-catalyzed azide-alkyne cycloaddition (CuAAc) obtaining the peptide-functionalized squaramide monomers **2** (Scheme S2.4). Monomers **1** and **2** were purified by high performance liquid chromatography (HPLC) prior to self-assembly and gel preparation. Detailed synthetic information can be found in the Supporting Information.

For subsequent 3D cell culture studies, a supramolecular co-assembly protocol was developed to mix both native monomer **1** and RGD-functionalized squaramide monomer **2** (Scheme 2.1A and Figure S2.1). DMSO stock solutions of monomers **1** and **2** were first prepared at concentrations of 25 mM and 5 mM, respectively, followed by mixing in a controlled and tunable manner based on concentration and volume calculations. The DMSO mixture was then exposed to nitrogen flow overnight to obtain a dried film. Afterwards, hydrogel preparation was performed by rehydration in PBS, vortexing, and sonication in an ice-water bath (4°C, ~ 30 min). Lastly, the obtained transparent solution was incubated at 37°C for 30 min and equilibrated overnight prior to further use for subsequent experiments.

UV-Vis spectroscopy measurements were performed to understand the effect of the mixing protocol on the functional squaramide-based supramolecular monomers and mixtures at the molecular level. UV-Vis spectra of both monomer **1** and **2** in DMSO showed a single band at 293 nm that consistent with depolymerization of the squaramide monomers (Figure S2.1).[29] After rehydration of the films in PBS, samples containing 2, 5, 10 and 15 mol% of monomer **2** (SQ-2RGD, SQ-5RGD, SQ-10RGD and SQ-15RGD) displayed two absorption bands at 262 nm and 322 nm corresponding to the HOMO−LUMO+1 and HOMO−LUMO transitions of squaramide, respectively (Figure S2.5).[29][31] These bands are identical to the supramolecularly polymerized monomer **1**

44

on its own suggesting that the mixing of monomer **2** up to 15 mol% does not modify its aggregation at the molecular level. However, further increasing the amount of monomer **2** up to 40 mol%, the HOMO−LUMO+1 and HOMO−LUMO transitions were recorded at 267 nm and 319 nm, pointing to a slightly lower degree of aggregation compared to the native monomer **1**. Together these results suggest DMSO depolymerizes the squaramide monomers, including those with the RGD peptide functionality, and repolymerization is achieved when prepared as co-assemblies in buffered solutions.
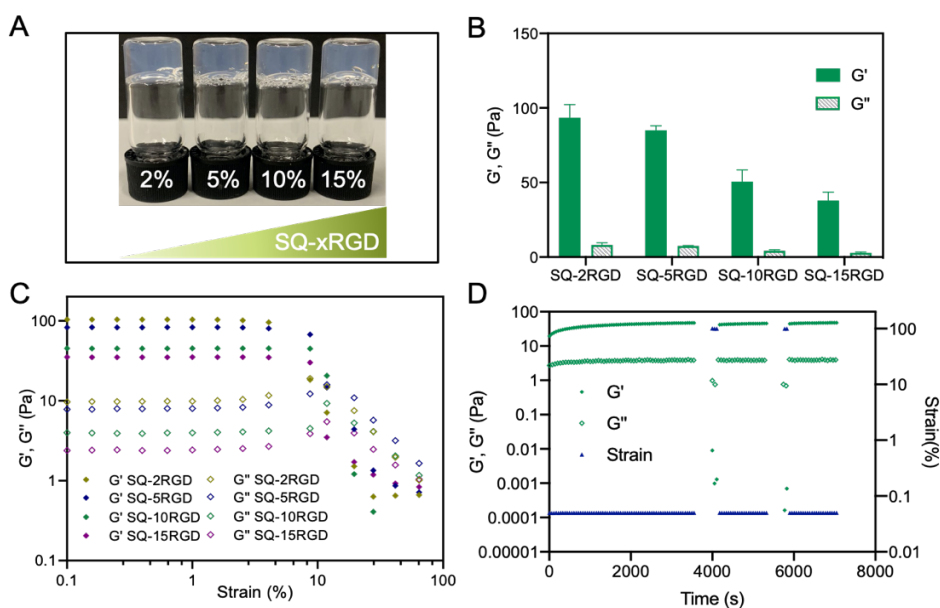
Figure 2.1. A) Gel inversion test of RGD-functionalized squaramide hydrogels (3.1 mM) prepared in PBS (pH 7.4) SQ-xRGD: hydrogels containing x mol% of the monomer **2**. Oscillatory rheology measurements: B) Averaged (N = 3) storage (G') and loss (G'') moduli of hydrogels (3.1 mM, PBS) collected at 37 ± 0.2˚C by a time-sweep measurement with a fixed frequency of 1 Hz and strain of 0.05%. C) Amplitude sweep of RGD-functionalized squaramide hydrogels at 37 ± 0.2˚C with a frequency of 1 Hz and strain from 0.1% to 100%. D) Step-strain measurements of hydrogel SQ-10RGD (3.1 mM) at 37 ± 0.2˚C with a frequency of 1 Hz. Frequency-sweep measurements (from

0.01 to 2 Hz, γ = 0.05%) were performed between application of low (0.05%) and high strain (100%) (Data was not show in this graph).

Physicochemical properties of bioactive squaramide-based supramolecular materials.
RGD-functionalized squaramide hydrogels were prepared with various mol% of monomer **2** and their capacity to gelate water was first approximated by a gel inversion test. The total squaramide monomer concentration was maintained at 3.1 mM and the effect of increasing the amount of monomer **2** on co-assembly was examined (0.06 - 0.45 mM RGD peptides) (Figure 2.1A). Non-flowing hydrogel materials were observed up to 15 mol% **2**. The mechanical properties of RGD-functionalized squaramide hydrogels were further assessed quantitatively by performing oscillatory rheology. From the time sweep measurements, hydrogel formation was confirmed with storage moduli (G') being greater loss moduli (G'') for the various samples. Mechanically soft hydrogels were formed for all compositions with a G' lower than 100 Pa; a decreasing trend was observed with the increase of monomer **2** (Figure 2.1B). An amplitude sweep experiment in a range of strain from 0.1% to 100% was used to determine the linear viscoelastic (LVE) region of the various materials. In the case of hydrogels SQ-2RGD and SQ-5RGD, G' and G'' remained constant until 4% strain, whereas for hydrogels SQ-10RGD and SQ-15RGD the exit from the linear regime was observed at 6% strain (Figure 2.1C). Moreover, frequency sweep measurements showed rheological profiles consistent with viscoelastic materials in a frequency range from 0.01 Hz to 2 Hz for all hydrogels up to 15 mol% monomer **2** with G' was greater than G'' by an order of magnitude (Figure S2.2). Lastly, step-strain measurements were executed to evaluate the effect of the added monomer **2** on the self-recovery properties of the supramolecular hydrogels. With the addition of monomer **2** up to 15 mol%, the RGD-functionalized squaramide hydrogels showed similar self-recovery behavior to the previously reported native hydrogel SQ, namely the decrease and inversion of both moduli (G' and G") in response to large amplitude strain, and recovery of the material

to its initial state after its removal over two cycles (Figure 2.1D and S2.3).[31] To better understand the effect of increasing peptide monomer concentration, a sample with a greater mol percentage of monomer **2** (SQ-40RGD) was examined. While G' > G" in time sweep measurements, G' and G" were found to decrease (G' = 1.26 Pa, G" = 0.27 Pa) significantly (Figure S2.4) demonstrating a negative effect of the peptide monomer on gelation properties.

Further insight into the origin of the measured rheological properties was provided by cryogenic transmission electron microscopy (cryo-TEM). As shown in Figure S2.5, flexible, micron-length nanofibers were observed for SQ-10RGD hydrogels (3.1 mM, PBS) indistinguishable from the SQ hydrogels with a slightly smaller width of 4.8 ± 0.4 nm. Because of the difference in gel rheological properties with increasing peptide concentration, we further examined the effect of increasing monomers **2** on the nanoscale structure of the squaramide-based supramolecular polymer fibres. Similarly, entangled fibers were observed in SQ-40RGD solution, with comparable fibre width of 4.6 ± 0.6 nm, indicating that the co-assembly of monomer **2** was comparable at the nanoscale level (Figure S2.6).

Encapsulated NIH3T3-mCherry-LifeAct cells recognize RGD peptides in the supramolecular network and migrate. RGD peptides bind cell-surface integrins and through these receptors they stimulate actin polymerization upon cell attachment, facilitating cell spreading and contractile movements.[34,35] Therefore, before applying the co-assembled supramolecular polymers for 3D cell culture, we first investigated whether cells can recognize and respond to the RGD peptides presented by the squaramide-based polymers. Consequently, NIH3T3-LifeAct-mCherry cells transduced to express m-Cherry-labelled actin were encapsulated and cultured in squaramide-based hydrogels. Branched, large protrusions (pseudopods) tipped with actin rich filopodia outside of the cell body were observed in the SQ-10RGD and SQ-15RGD hydrogels, as previously reported in ECM-derived collagen hydrogels (Video S2.1 and

S2.2). [36,37] Additional to protrusion formation, cell migration was also observed indicating extensive cell-hydrogel interactions in 3D. In contrast, cells in native SQ hydrogels displayed a highly rounded morphology, with minimal spreading and were rarely observed to migrate (Video S2.3). This indicates that the inclusion of RGD peptides is essential for cell spreading and migration in the squaramide-based supramolecular hydrogel. To further quantify cell spreading efficiency as a function of RGD concentration, cells were cultured in squaramide-based hydrogels for 24h and then subsequently imaged (2.5 µm stepped z-stacks). Using image analysis, all cells in each imaged volume slice were recognized and a local two-dimensional z-projection was made around each cell to individually analyze and extract appropriate cell edges. The cell edges were used to calculate morphological parameters such as cell area, perimeter, circularity, summated skeleton branch length, min- and max Feret diameter and aspect ratio. Cells tended to spread significantly more in RGD-functionalized squaramide hydrogels, as shown in Figure 2.2A and S2.8, and quantitatively displayed larger cell areas and longer perimeters in comparison to those in SQ (P<0.001, Figure 2.2B and S2.8). Consistently, cell circularity was much lower in RGD-functionalized hydrogels, calculated to be 0.726, 0.619 and 0.694 for cells in SQ-5RGD, SQ-10RGD and SQ-15RGD, respectively, in comparison to that in SQ (0.903). To gather further information of cell protrusion formation, the cell shapes were skeletonized, the Feret diameters were measured and aspect ratios were calculated. Significantly larger Feret diameters were observed for cells cultured in RGD-functionalized hydrogel in comparison to that in SQ (P<0.001), supporting cell elongation within the RGD-presenting materials. Among them, the lowest aspect ratio was calculated from cells cultured in SQ-10RGD, as shown in Figure 2.2B. Moreover, the summated skeleton branch lengths for each cell, used as an indicator of protrusion length, was found to be 22.4 ± 3.3 µm in SQ-10RGD, a 4-fold increase over that in SQ (5.2 ± 1.2 µm) (Figure 2.2B and Table S2.1). Taken together, the cells displayed a more spread and branched morphology with highly dynamic actin polymerization along the cell membrane,

especially at the end of branched protrusions as a consequence of interaction with RGD peptides in the bioactive squaramide-based hydrogels as previously reported in literature powering cell migration within the hydrogels.[34]
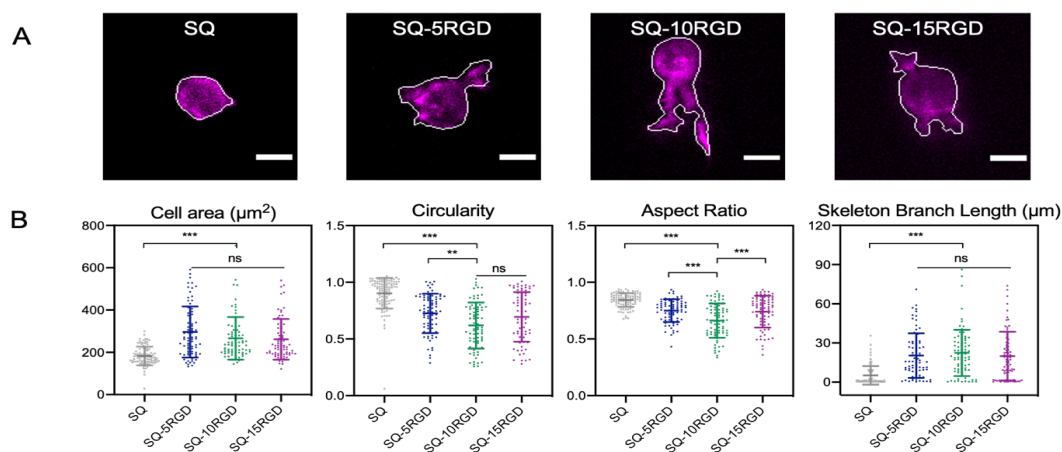
Figure 2.2. A) Representative images of NIH3T3-LifeAct-mCherry cells cultured within squaramide-based hydrogels after 24h, scale bar: 10 µm; B) Quantitative analysis of mean projected cell area, perimeter, circularity and skeleton branch length from NIH3T3-mCherry-LifeAct cells cultured for 24h within squaramide-based hydrogel. For each data set, 74-100 cells were analyzed. The mean and standard deviation are marked within the graphs. (*P< 0.05, **P< 0.01, ***P< 0.001 one-way Anova)

Impact of the RGD-functionalized squaramide hydrogels on HepG2 spheroids formation and growth. The aggregation of HepG2 cells into spheroidal structures that resemble their presentation *in vivo* provide a versatile tool to investigate hepatic metabolism, stemness, cancer and chemical safety assessment.[38–40] Because bioactive squaramide-based hydrogels containing an RGD-ligand support active cell migration and proliferation, we became interested if these materials would further enable the self-assembly of HepG2 cells into spheroids and facilitate their differentiation. A recent study demonstrated that low concentrations of RGD peptide (~0.2 mM) may be not sufficient for human liver organoid proliferation,[17] thus bioactive squaramide-based hydrogels were examined at 0.3 and 0.45 mM RGD with hydrogels lacking the RGD

monomer **2** and Matrigel being used as controls. As expected, HepG2 cells grew within SQ-10RGD hydrogel by starting from single cells (1 x 10^5 cells/mL) on day 3 to small aggregates on day 7, and finally, rounded spheroids on day 14 that continued to increase slightly in size until day 21 (Figure 2.3A). HepG2 cells grew similarly in SQ and SQ-15RGD hydrogels forming compact spheroids on day 14. As a control, spheroids cultured in Matrigel, the current gold standard cell culture matrix, displayed a slightly less compacted morphology throughout the culture period. Spheroid diameter was measured to quantitatively compare the performance of the supramolecular matrix against Matrigel in generating these morphological structures. Increase in the spheroidal diameter over the 21-day culture period was confirmed by plotting the measured size distributions in Figure 2.3B. Cellular aggregates of 58 ± 18, 69 ± 17 and 64 ± 17 µm were obtained on day 7 in SQ, SQ-10RGD and SQ-15RGD hydrogels, and grew into spheroids with diameters of 116 ± 40 µm, 112 ± 32 µm, and 129 ± 49 µm on day 14, respectively. From day 14 to day 21, spheroids in SQ and SQ-10RGD hydrogels were comparable in diameter, 127 ± 30 µm and 119 ± 30 µm, respectively. Conversely, HepG2 cells cultured in Matrigel formed spheroids with average diameter of 102 ± 31 µm on day 7 and increased in size to 128 ± 40 µm on day 14 and 122 ± 22 µm on day 21, respectively. From all hydrogel conditions tested, the HepG2 spheroids in SQ-15RGD hydrogel displayed highest diameters at 163 ± 66 µm on day 21, yet remained below 200 µm providing sufficient oxygen diffusion throughout the spheroid.[41,42] This increase in spheroid diameter in the squaramide-based hydrogels suggests proliferation of HepG2 cells during the culture period.
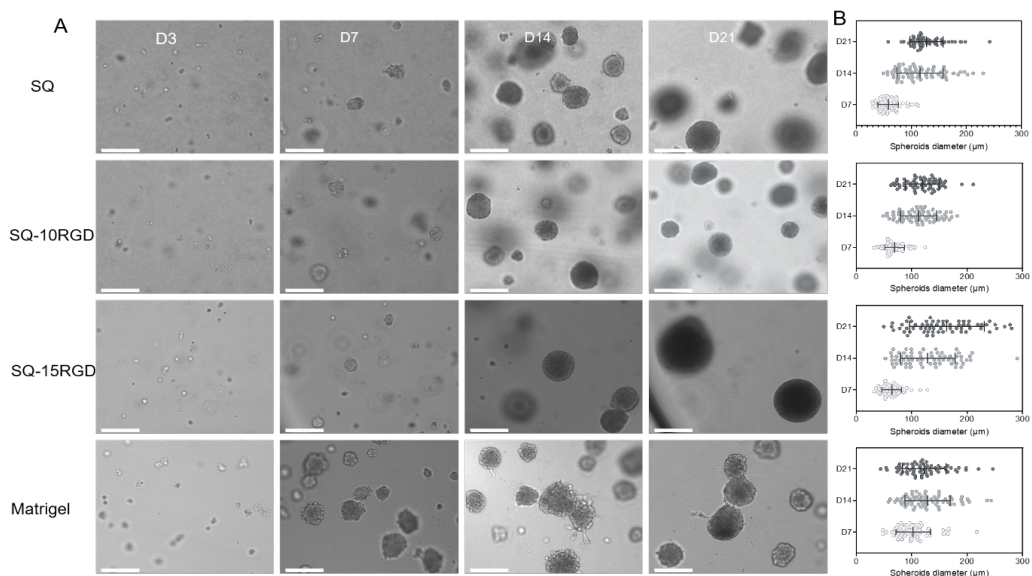
Figure 2.3. 3D HepG2 cell culture in squaramide-based hydrogels over a 21-day period. A) Bright field images taken on day 3 (D3), 7 (D7), 14 (D14) and 21 (D21). Scale bar: 200 μm. B) Size distribution of HepG2 spheroids during the 21-day culture period in squaramide-based hydrogels and Matrigel (LOT5215008). For each group, 66 spheroids were measured in Fiji by manually drawing a straight line horizontally (angle < 3°). The means and standard deviations are marked inside the graphs.

Proliferation of the HepG2 spheroids cultured in the bioactive squaramide-based hydrogels were further assessed by their imaging with 5-ethynyl-2'-deoxyuridine (EdU). In order to facilitate their staining, the HepG2 spheroids were released from the hydrogels by dilution of the supramolecular matrix at pre-determined time points, imaged and analyzed quantitatively for EdU positive cells. Proliferative cells were observed to be randomly distributed throughout the HepG2 spheroids suggesting that sufficient nutrient diffusion through squaramide-based hydrogels and the spheroids occurs during culture (Figure 2.4B). In the SQ hydrogel lacking RGD peptides, HepG2 cells displayed comparable proliferative activity based on the EdU-positive percentage over the culture period, namely 18 ± 16.2% on day 7, 8 ± 6.4% on day 14 and 10 ± 6.2% on day 21, respectively. In the RGD-functionalized squaramide-based hydrogel, HepG2

cells were found to proliferate actively at the beginning of the culture period with the measured percentage of EdU-positive cells on day 7 being 25 ± 9.9% and 45 ± 8.4% in SQ-10RGD and SQ-15RGD hydrogels, respectively. Notably, HepG2 cells cultured in Matrigel displayed an EdU-positive percentage of 41 ± 12.8% on day 7 that declined to 7 ± 5.0% on day 14 and eventually ended at 6 ± 5.2%. As the culture progressed from day 7 to 14 in both Matrigel and squaramide hydrogels, a dramatic decrease in the percentage of EdU-positive cells was measured pointing to decreased proliferation and suggestive of their differentiation. SQ-15RGD showed the highest proliferation of the HepG2 cells in comparison to Matrigel, SQ and SQ-10RGD hydrogels on day 14, and is consistent with the significantly larger measured diameter of the spheroids. In the case of SQ-10RGD and SQ-15RGD slightly increased proliferation of 13 ± 9.2% and 14 ± 2.8%, respectively, was recorded at the end of culture and is slightly greater than for the SQ monomer (10 ± 6.2%) (Figure 2.4C and S2.10). Besides the early active cell proliferation, HepG2 spheroids cultured within squaramide-based hydrogels were largely calcein AM positive with few dead cells confirming high cell viability and the absence of a necrotic core during the culture (Figure 2.4A and S2.9). Collectively, RGD-functionalized squaramide hydrogels support the formation of HepG2 spheroids with a size greater than 150 µm initially showing active cell proliferation that decreases towards the end of the 21-day culture period. The initial increased cell proliferation could further affect HepG2 cell differentiation resulting in the induction of metabolic enzymes and expression of hepatic markers.
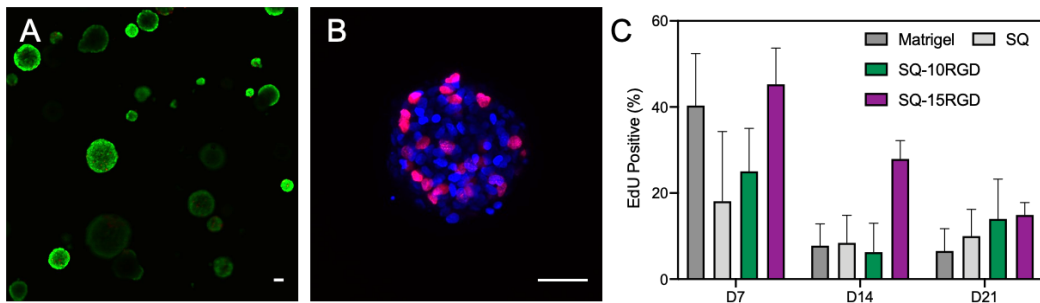
Figure 2.4. A) Cell viability assay of HepG2 spheroids cultured in SQ-10RGD hydrogel for 21 days stained by a LIVE/DEAD assay with calcein AM (viable cells, *green*) and propidium iodide (PI) (dead cells, *red*). B) EdU staining of released HepG2 spheroids cultured in SQ-10RGD hydrogels. Proliferating cells were labelled with EdU-Alexa fluor 594 (*red*) and cell nuclei were stained with Hoechst 33342 (*blue*). Scale bar: 50 µm. C) Quantification of EdU percentage in HepG2 spheroids cultured within Matrigel, SQ, SQ-10RGD and SQ-15RGD hydrogels. N=3.

Improved metabolic enzyme and hepatic marker expression of HepG2 spheroids after culture in RGD-functionalized squaramide hydrogels. HepG2 cells showed spheroid formation in SQ, SQ-10RGD and SQ-15RGD hydrogels with high cell viability and increased proliferation in the bioactive gels early on in the culture. However, it was previously demonstrated that the formation of these *in vivo* mimicking structures in 3D in peptide nanofiber hydrogel-based does not necessarily result in the distinct expression of metabolizing enzymes by RT-PCR. [11] Consequently, to assess the bioactive squaramide-based materials on the maturation of HepG2 spheroids, RT-PCR experiments were performed to evaluate the expression of a panel of metabolic enzymes and hepatic markers. As hypothesized, the HepG2 spheroids showed higher expression of various phase I and II metabolic enzymes and drug transporters in the 3D cultures performed in comparison to 2D (Figure 2.5A). mRNA expression of CYP1A2 measured from cells cultured in 3D in the Matrigel matrix control was over 40-fold in

comparison to the 2D condition. Similarly, both CYP2C19 and CYP3A4 showed an over 10-fold enhancement in 3D in comparison to 2D culture and CYP2C9 and CYP2D6 expression was increased 3- and 4.5-fold, respectively. Additionally, mRNA levels of the phase II xenobiotic-metabolizing enzymes UGT1A1 increased by over 45-fold and expression of hepatic markers HNF4a and NCTP were also found to increase over two times during hydrogel-based culture. The overall higher gene expression of metabolic enzymes and hepatic markers are consistent with previous reports that the formation of compact spheroids in 3D are beneficial for hepatocyte maturation.[8,12] When compared against the HepG2 spheroids cultured in Matrigel, cells cultured in the bioactive squaramide-based hydrogel SQ-10RGD in 3D displayed significantly higher mRNA expression in case of CYP2D6 (4.7-fold), CYP2C19 (4.2-fold), CYP2C9 (3.6-fold), and NCTP (4.9-fold) and comparable level in CYP1A2 (1.8-fold), UGT1A1 (1.4-fold), CYP3A5 (1.5-fold), and HNF4a (1.5-fold). These results strongly suggest that the fully synthetic bioactive squaramide-based hydrogel can function well as an alternative matrix of Matrigel for HepG2 culture. More importantly, in comparison to the control SQ hydrogel, cells were cultured within SQ-10RGD hydrogel displayed significant improved mRNA expression of NCTP (**P<0.01) and advantageous expression of CYP2D6, CYP2C19, CYP1A2, HNF4a and UGT1A1, confirming the importance of incorporating bioactive peptides to further stimulate differentiation. The overall enhancement in gene expression in HepG2 spheroids by introducing RGD peptides is less obvious than that of transferring cells from 2D to 3D culture, implying cell-cell contact plays a critical role in their differentiation rather than cell-matrix interactions, at least under the tested cell seeding condition.[43,44] However, matrix proteins have been earlier demonstrated to play an important role in the assembly of HepG2 spheroids and this can also explain the subtle increases between the RGD and native conditions.[45]

To further probe the differentiation of spheroids in 3D in squaramide-based hydrogels, immunostaining of albumin and bile canaliculi-like structures through MRP2 was performed (Figure 2.5B and S2.12).[8,9] Albumin expression was present in both Matrigel and squaramide-based hydrogels culture systems. In contrast, MRP2 expression was localized in actin-rich regions suggesting bileduct formation, with a more intense staining in hepG2 spheroids that were cultured in SQ and SQ-10RGD hydrogels in comparison to those in Matrigel. Conversely, MRP2 staining was hardly observed in spheroids from the SQ-15RGD hydrogel that had the largest aggregates. Moreover, β-catenin expression at the borders of the hepG2 spheroids indicate that independent of the gel used the cells establish basal-lateral polarity.

To summarize, the quantified mRNA expression of metabolic enzymes and hepatic makers from HepG2 cells cultured in squaramide-based hydrogels confirms our hypothesis that our bioactive and chemical-defined synthetic matrix can be an alternative to Matrigel to support their 3D cell culture, and importantly, incorporation of cell adhesion motifs (RGD) enhanced cell proliferation and thus improve cell hepatic makers expression in 3D. Still, as observed from real-time PCR analysis in Figure 2.5A, some variation between biological replicates was observed in the gene expression, which was comparable to that of Matrigel from different lots (Figure S2.11), especially with respect to CYP1A2 and UGT1A1 expression. Likely these variations are due to the non-uniform size of the formed spheroids in 3D within the materials that influence the metabolic activity of the HepG2 cells and further refinement of the overall synthetic matrix composition and/or culture protocol will require methods to control spheroid size prior to cell culture within the materials.[46,47] Gratifyingly, this fully synthetic supramolecular squaramide–based matrix can support HepG2 early proliferation and differentiation with the expression of several key metabolic enzymes and hepatic markers to a greater extent than Matrigel.
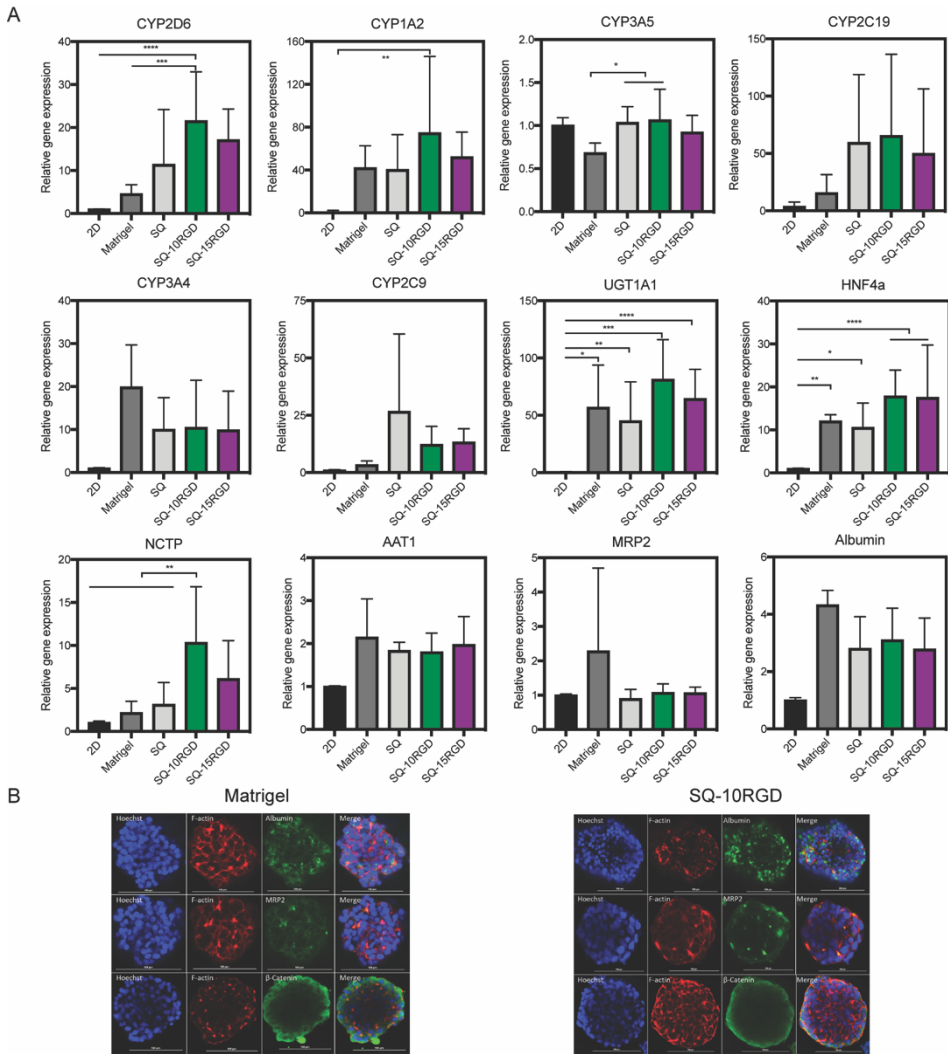
Figure 2.5. A) Real-time PCR analysis of metabolic enzymes and liver-specific markers in 2D and 3D culture. Fold change gene expression levels of spheroids after a 21-day 3D culture compared to 3-day 2D cultured HepG2 cells. Data are collected from three biological replicates (*P< 0.05, **P< 0.01, ***P< 0.001, ****P< 0.0001 one-way Anova). B) Immunofluorescence staining of the liver markers albumin (upper row), MRP2 (middle row) and β-catenin (lower row) in green, and counter-stained with F-actin rhodamine phalloidin (*red*) and the nuclear stain Hoechst33342 (*blue*). Merged channels consist of all three stainings. Scale bar: 100 μm.

2.4 Conclusions

A fully synthetic and bioactive squaramide-based supramolecular hydrogel material bearing RGD peptides was prepared for 3D cell culture. The co-assembly approach of the synthesized monomers **1** and **2** to prepare the hydrogel materials enables tuning of the peptide concentration within the materials. The RGD-functionalized squaramide-based hydrogels were demonstrated to be optically clear, mechanically soft and self-recovering. Encapsulated cells recognize the RGD peptides (0.15-0.45 mM) embedded within the network by spreading, initiating actin polymerization and inducing cell migration in 3D. These RGD-functionalized squaramide hydrogels support the growth of HepG2 cells into compact spheroids with high cell viability, active proliferation and differentiation, resulting in significantly higher gene expression of metabolic enzymes and hepatic markers as well as the formation of liver structures and basal-lateral polarization. This chemically well-defined monomers enable a facile preparation protocol through their co-assembly, cytocompatibility and capacity to trigger differentiation on par with natural materials challenging Matrigel, the current gold standard for liver spheroid culture, but can be more broadly applied in other areas of tissue culture where cell-matrix interactions are necessary to facilitate various aspects of cell behaviour. Moreover, their self-recovering properties enable gentle spheroid release which can be used for downstream analysis. Finally, the terminal azide on squaramide monomer **3** leaves the door open to further chemically modification and crosslinks for future biomaterials designs, e.g. tuning the stiffness of supramolecular network in a straightforward manner to provide a closer *in vivo* mimicking microenvironment for cells.

2.5 References

[1]   O. A. Almazroo, M. K. Miah, R. Venkataramanan, *Clin. Liver Dis.* **2017**, *21*, 1.

[2]   R. J. Andrade, G. P. Aithal, E. S. Björnsson, N. Kaplowitz, G. A. Kullak-Ublick, D.

Larrey, T. H. Karlsen, *J. Hepatol.* **2019**, *70*, 1222.

[3]   G. A. Kullak-Ublick, R. J. Andrade, M. Merz, P. End, A. Benesic, A. L. Gerbes, G. P. Aithal, *Gut.* **2017**, *66*, 1154.

[4]   J. A. Heslop, C. Rowe, J. Walsh, R. Sison-Young, R. Jenkins, L. Kamalian, R. Kia, D. Hay, R. P. Jones, H. Z. Malik, S. Fenwick, A. E. Chadwick, J. Mills, N. R. Kitteringham, C. E. P. Goldring, B. Kevin Park, *Arch. Toxicol.* **2017**, *91*, 439.

[5]   C. Rowe, D. T. Gerrard, R. Jenkins, A. Berry, K. Durkin, L. Sundstrom, C. E. Goldring, B. K. Park, N. R. Kitteringham, K. P. Hanley, N. A. Hanley, *Hepatology* **2013**, *58*, 799.

[6]   H. H. J. Gerets, K. Tilmant, B. Gerin, H. Chanteux, B. O. Depelchin, S. Dhalluin, F. A. Atienzar, *Cell Biol. Toxicol.* **2012**, *28*, 69.

[7]   C. S. Hughes, L. M. Postovit, G. A. Lajoie, *Proteomics.* **2010**, *10*, 1886.

[8]   S. C. Ramaiahgari, M. W. Den Braver, B. Herpers, V. Terpstra, J. N. M. Commandeur, B. Van De Water, L. S. Price, *Arch. Toxicol.* **2014**, *88*, 1083.

[9]   S. Hiemstra, S. C. Ramaiahgari, S. Wink, G. Callegaro, M. Coonen, J. Meerman, D. Jennen, K. van den Nieuwendijk, A. Dankers, J. Snoeys, H. de Bont, L. Price, B. van de Water, *Arch. Toxicol.* **2019**, *93*, 2895.

[10]   K. R. Stevens, J. S. Miller, B. L. Blakely, C. S. Chen, S. N. Bhatia, *J. Biomed. Mater. Res. -Part A* **2015**, *103*, 3331.

[11]   M. M. Malinen, H. Palokangas, M. Yliperttula, A. Urtti, *Tissue Eng. - Part A* **2012**, *18*, 2418.

[12]   H. Jeon, K. Kang, S. A. Park, W. D. Kim, S. S. Paik, S. H. Lee, J. Jeong, D. Choi, *Gut Liver* **2017**, *11*, 121.

[13]   N. S. Bhise, V. Manoharan, S. Massa, A. Tamayol, M. Ghaderi, M. Miscuglio, Q. Lang, Y. S. Zhang, S. R. Shin, G. Calzone, N. Annabi, T. D. Shupe, C. E. Bishop, A. Atala, M. R. Dokmeci, A. Khademhosseini, *Biofabrication* **2016**, *8*, 014101.

[14]   J. Christoffersson, C. Aronsson, M. Jury, R. Selegård, D. Aili, C. F. Mandenius, *Biofabrication* **2019**, *11*, 015013.

[15]   M. Krüger, L. A. Oosterhoff, M. E. van Wolferen, S. A. Schiele, A. Walther, N. Geijsen, L. De Laporte, L. J. W. van der Laan, L. M. Kock, B. Spee, *Adv. Healthc. Mater.* **2020**, *9*, 1901658.

[16] B. J. Klotz, L. A. Oosterhoff, L. Utomo, K. S. Lim, Q. Vallmajo-Martin, H. Clevers, T. B. F. Woodfield, A. J. W. P. Rosenberg, J. Malda, M. Ehrbar, B. Spee, D. Gawlitta, *Adv. Healthc. Mater.* **2019**, *8*, 1900979.

[17] S. Ye, J. W. B. Boeter, M. Mihajlovic, F. G. van Steenbeek, M. E. van Wolferen, L. A. Oosterhoff, A. Marsee, M. Caiazzo, L. J. W. van der Laan, L. C. Penning, T. Vermonden, B. Spee, K. Schneeberger, *Adv. Funct. Mater.* **2020**, *2000893.*

[18] G. Sorrentino, S. Rezakhani, E. Yildiz, S. Nuciforo, M. H. Heim, M. P. Lutolf, K. Schoonjans, *Nat. Commun.* **2020**, *11*, 1.

[19] M. Kumar, B. Toprakhisar, M. Van Haele, A. Antoranz, R. Boon, bioRxiv **2020**. 280883.

[20] M. J. Webber, E. A. Appel, E. W. Meijer, R. Langer, *Nat. Mater.* **2015**, *15*, 13.

[21] C. L. Maikawa, A. A. A. Smith, L. Zou, G. A. Roth, E. C. Gale, L. M. Stapleton, S. W. Baker, J. L. Mann, A. C. Yu, S. Correa, A. K. Grosskopf, C. S. Liong, C. M. Meis, D. Chan, M. Troxell, D. M. Maahs, B. A. Buckingham, M. J. Webber, E. A. Appel, *Nat. Biomed. Eng.* **2020**, *4*, 507.

[22] D. Straßburger, N. Stergiou, M. Urschbach, H. Yurugi, D. Spitzer, D. Schollmeyer, E. Schmitt, P. Besenius, *ChemBioChem.* **2018**, *19*, 912.

[23] S. Spaans, P. P. K. H. Fransen, M. J. G. Schotman, R. Van Der Wulp, R. P. M. Lafleur, S. G. J. M. Kluijtmans, P. Y. W. Dankers, *Biomacromolecules.* **2019**, *20*, 2360.

[24] Y. Wang, K. M. Dillon, Z. Li, E. W. Winckler, J. B. Matson, *Angew. Chemie.* **2020**, 16841.

[25] J. Ramos, S. Arufe, H. Martin, D. Rooney, R. B. P. Elmes, A. Erxleben, R. Moreira, T. Velasco-Torrijos, *Soft Matter.* **2020**, *16*, 7916.

[26] L. A. Marchetti, L. K. Kumawat, N. Mao, J. C. Stephens, R. B. P. Elmes, *Chem.* **2019**, *5*, 1398.

[27] C. López, M. Ximenis, F. Orvay, C. Rotger, A. Costa, *Chem. - A Eur. J.* **2017**, *23*, 7590.

[28] E. Castellanos, B. Soberats, S. Bujosa, C. Rotger, R. De Rica, A. Costa, *Biomacromolecules.* **2020**, *21*, 966.

[29] V. Saez Talens, P. Englebienne, T. T. Trinh, W. E. M. Noteborn, I. K. Voets, R. E.

Kieltyka, *Angew. Chemie.* **2015**, *127*, 10648.

[30]   V. Saez Talens, D. M. M. Makurat, T. Liu, W. Dai, C. Guibert, W. E. M. Noteborn, I. K. Voets, R. E. Kieltyka, *Polym. Chem.* **2019**, *10*, 3146.

[31]   C. Tong, T. Liu, V. Saez Talens, W. E. M. Noteborn, T. H. Sharp, M. M. R. M. Hendrix, I. K. Voets, C. L. Mummery, V. V. Orlova, R. E. Kieltyka, *Biomacromolecules.* **2018**, *19*, 1091.

[32]   V. Saez Talens, G. Arias-Alpizar, D. M. M. Makurat, J. Davis, J. Bussmann, A. Kros, R. E. Kieltyka, *Biomacromolecules.* **2020**, *21*, 1060.

[33]   K. D. Park, R. Liu, H. Kohn, *Chem. Biol.* **2009**, *16*, 763.

[34]   C. H. Yu, J. B. K. Law, M. Suryana, H. Y. Low, M. P. Sheetz, *Proc. Natl. Acad. Sci. U. S. A.* **2011**, *108*, 20585.

[35]   P. T. Caswell, T. Zech, *Trends Cell Biol.* **2018**, *28*, 823.

[36]   K. M. Hakkinen, J. S. Harunaga, A. D. Doyle, K. M. Yamada, *Tissue Eng. - Part A* **2011**, *17*, 713.

[37]   H. Liu, M. Wu, Y. Jia, L. Niu, G. Huang, F. Xu, *NPG Asia Mater.* **2020**, *12*, 45.

[38]   F. van Zijl, W. Mikulits, *World J. Hepatol.* **2010**, *2*, 1.

[39]   S. E. Kim, S. Y. An, D. H. Woo, J. Han, J. H. Kim, Y. J. Jang, J. S. Son, H. Yang, Y. P. Cheon, J. H. Kim, *Stem Cells Dev.* **2013**, *22*, 1818.

[40]   D. S. Reynolds, K. M. Tevis, W. A. Blessing, Y. L. Colson, M. H. Zaman, M. W. Grinstaff, *Sci. Rep.* **2017**, *7*, 1.

[41]   A. Asthana, W. S. Kisaalita, *Drug Discov. Today* **2012**, *17*, 810.

[42]   X. Cui, Y. Hartanto, H. Zhang, *J. R. Soc. Interface* **2017**, *14*, 20160877.

[43]   T. A. Brieva, P. V. Moghe, *Biotechnol. Bioeng.* **2004**, *85*, 283.

[44]   R. Z. Lin, L. F. Chou, C. C. M. Chien, H. Y. Chang, *Cell Tissue Res.* **2006**, *324*, 411.

[45]   R. Akasov, D. Zaytseva-Zotova, S. Burov, M. Leko, M. Dontenwill, M. Chiper, T. Vandamme, E. Markvicheva, *Int. J. Pharm.* **2016**, *506*, 148.

[46]   Y. Miyamoto, M. Ikeuchi, H. Noguchi, T. Yagi, S. Hayashi, *Cell Med.* **2015**, *8*, 47.

[47]   T. Nishikawa, Y. Tanaka, M. Nishikawa, Y. Ogino, K. Kusamori, N. Mizuno, Y. Mizukami, K. Shimizu, S. Konishi, Y. Takahashi, Y. Takakura, *Biol. Pharm. Bull.*

2017, *40*, 334.

2.6 Supporting Information

2.6.1 Materials

All chemicals used in the synthesis of monomers **1** and **2** were purchased from Sigma Aldrich and used without further purification. Fmoc-protected amino acids for peptide synthesis were obtained from Novabiochem. Dulbecco's modified eagle cell culture medium (DMEM), DMEM/F12, fetal calf serum, penicillin, streptomycin, GlutaMAX, pyruvate and trypsin were received from Thermo Fisher Scientific. Angiogenesis slides (15-well) were obtained from Ibidi. Dulbecco's Phosphate Buffered Saline (DPBS), calcein AM (AM = acetoxymethyl), and propidium iodide (PI) were acquired from Sigma-Aldrich. The Click-iT EdU Imaging kit was purchased from Invitrogen. Total RNA Isolation (TRI) Reagent was from Sigma-Aldrich. RevertAid H Minus First Strand cDNA Synthesis Kit and PowerUp™ SYBR™ Green Master Mix were obtained from Thermo Fisher Scientific.

2.6.2 Instruments

All synthetic intermediates were characterized by ^{1}H-NMR and ^{13}C-NMR collected on a Bruker DMX-400 operating at 400 MHz and 100 MHz at 298 K, respectively. LC-MS analysis was performed on a TSQ Quantum Access MAX system equipped with a Gemini 3 μm C18 110 Å 50×4.60 mm column (UV detection at 214 nm and 254 nm, mass detection range: 160 to 3000 (Da)). The mobile phase consisted of a gradient of 10-90% of H_2O-CH_3CN with 0.1% trifluoroacetic acid (TFA) over 13.5 minutes. HPLC purification of the monomers was executed on setup equipped with C18 column. A gradient from 10%-90% CH_3CN (0.1% TFA) in H_2O (0.1% TFA) over 15 min at a flow rate of 12 mL/min was used. Matrix-assisted laser desorption ionization-time-of-flight mass spectra (MALDI-TOF-MS) were collected on a Bruker Microflex LRF mass spectrometer on a ground steel target plate. A linear positive-ion mode with an α-cyano-4-

hydroxycinnamic acid matrix (5 mg/ml in CH_3CN/ H_2O 1:1 v/v) was used. High resolution mass spectra (HR-MS) were collected on a Thermo Fisher LTQ Orbitrap mass spectrometer equipped with an electrospray ion source in positive mode (resolution R = 60000). The spectra were collected by direct injection of samples (2 µM in H_2O-CH_3CN 50/50 v/v) and recorded with a mass range of 150-2000 and dioctylpthalate (m/z = 391.28428) as a "lock mass". Oscillatory rheology experiments were executed on a Discovery HR-2 hybrid rheometer using a cone-plate geometry (40 mm, 1.995°) at 37 ± 0.2 °C with a peltier-based temperature controller and solvent trap. Cryo-TEM images were acquired on a Tecnai F12 (FEI Company, The Netherlands) equipped with a field emission gun operating at 120 keV using a Gatan UltraScan charge-couple device (CCD) camera (Gatan company, Germany) with a defocus between −6 and −9 µm. UV absorption spectra were recorded on a Cary 300 Bio UV-Vis spectrometer, scanning from 200 nm to 400 nm with 1 nm intervals with a scan rate of 120 nm/min. Bright field images were taken on an EVOS FL AUTO2 equipped with temperature and a CO_2 gas controller. Confocal fluorescent images were acquired on Leica TCS SP8 confocal laser scanning microscope equipped with a 10× air objective and a 40× oil immersion objective. Images were processed using the Fiji Image J software. Real-time polymerase chain reaction (RT-PCR) measurements were performed on a QuantStudio™ 6 and 7 Flex Real-Time PCR (Applied Biosystems®).

2.6.3 Synthetic procedures
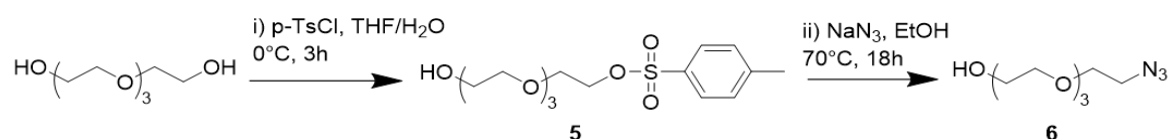
Scheme S2.1. Synthesis route for compound **6**.[1]

Compound 5. An aqueous NaOH (1.53 g, 38.25 mmol) solution (10 mL) was added to a solution of tetraethylene glycol (45.00 g, 231.68 mmol) dissolved in tetrahydrofuran

(THF) (10 mL) at 0°C. *p*-Toluenesulfonyl chloride (4.31 g, 22.61 mmol) dissolved in THF (30 mL) was added dropwise to the reaction mixture over 1h. After stirring at 0 °C for 2h, the reaction mixture was poured onto ice water (150 mL) and extracted 3x with DCM (200 mL). The combined organic layers were then washed with water (2 x 100 mL), dried with MgSO$_4$, and concentrated on a rotary evaporator. The crude was purified by column chromatography (petroleum ether (PE) /ethyl acetate (EtOAc) 60/40-0/100 v/v). The product was concentrated by rotary evaporation and dried in vacuum oven overnight to obtain a light yellow oil. Yield: 58%, 4.55 g. ^{1}H-NMR (CDCl$_3$, 400 MHz): 7.81-7.77 (d, 2H), 7.36-7.34 (d, 2H), 4.18-4.14 (m, 2H), 3.71-3.59 (m, 14H), 2.86 (s, 1H), 2.45 (s, 3H). ^{13}C-NMR (CDCl$_3$, 100 MHz): 144.88, 132.94, 129.87, 127.96, 72.51, 70.69, 70.63, 70.44, 70.30, 69.33, 68.66, 61.65, 21.65.

Compound 6. The obtained compound **5** (5.85 g, 16.80 mmol) was dissolved in ethanol (120 mL) and NaN$_3$ (2.79 g, 42.92 mmol) was added while stirring. The reaction mixture was then refluxed at 70 °C for 18h and water (100 mL) was added prior to concentrating the reaction mixture on a rotary evaporator. The concentrated solution was extracted with EtOAc (3 × 100 mL). The combined organic phases were dried over Na$_2$SO$_4$ and evaporated in vacuum to obtain compound **6** as a yellow oil. Yield: 77%, 2.83 g. ^{1}H-NMR (CDCl$_3$, 400 MHz): 3.71-3.58 (m, 14H), 3.40-3.36 (m, 2H), 3.13 (br s, 1H). ^{13}C-NMR (CDCl$_3$, 100 MHz): 72.47, 70.57, 70.54, 70.47, 70.21, 69.95, 61.51, 50.57.
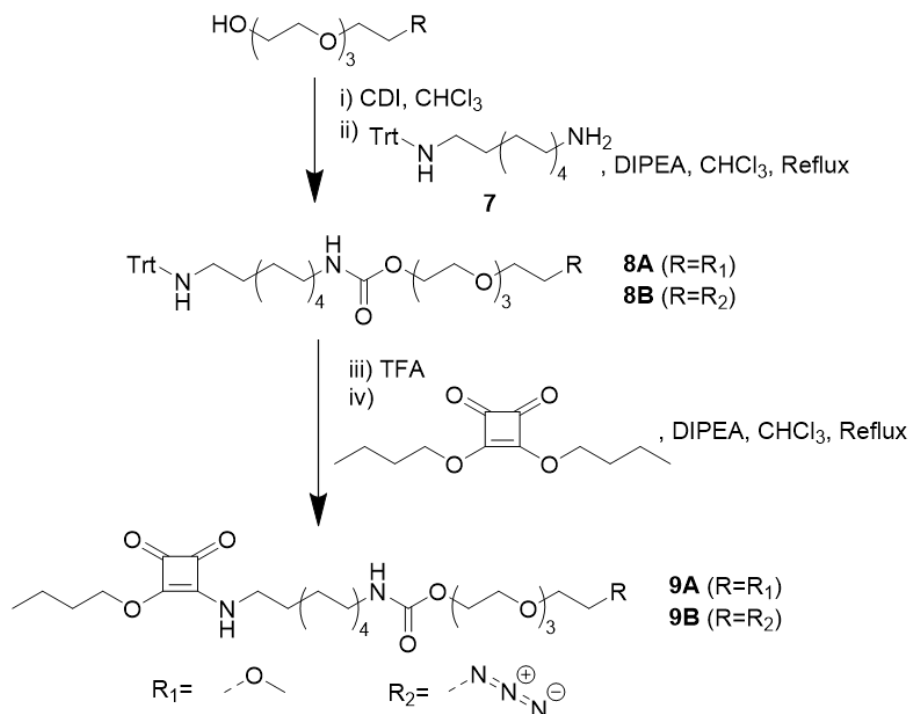
Scheme S2.2. Synthetic route for compound **9A** and **9B**.

Compound 7.[2] Triphenylmethyl chloride (2.73 g, 9.82 mmol) was dissolved in dichloromethane (DCM) (100 mL), added dropwise over 2h into a cooled (0°C), stirred solution of 1,10-diaminodecane (6.66 g, 38.65 mmol) in DCM (150 mL) and left to stir overnight at room temperature. Subsequently, the reaction mixture was concentrated by rotary evaporation and EtOAc (200 mL) was added before extracting with water (3 x 100 mL). The organic layer was collected, dried with anhydrous Na_2SO_4 and concentrated on a rotary evaporator. The crude was then purified by column chromatography (PE/EtOAC/methanol (MeOH) 50/50/0-50/50/20 v/v/v) and concentrated by rotary evaporation and dried in vacuum oven overnight to obtain a yellow oil. Yield: 79%, 3.20 g. ^{1}H-NMR (CDCl$_3$, 400 MHz): 7.51-7.48 (d, 6H), 7.26-7.22 (t, 6H), 7.19-7.12 (t, 3H), 2.70-2.64 (t, 2H), 2.16-2.10 (t, 2H), 1.51-1.44 (m, 4H), 1.33-1.02 (m, 12H). ^{13}C-NMR (CDCl$_3$, 100 MHz): 146.37, 128.65, 127.71, 126.12, 70.86, 43.56, 41.94, 33.19, 30.90, 29.64, 29.60, 29.58, 29.48, 27.37, 26.89. HR-MS: [M+H]$^+$: calcd: 415.3108, found: 415.3103.

Compound 8A. Tetraethyleneglycol monomethyl ether (0.90 g, 4.32 mmol) was activated with 1,1'-carbonyldiimidazole (CDI) (0.78 g, 4.81 mmol) for 1h at room temperature. Subsequently, compound **7** (2.19 g, 5.28 mmol), N,N-Diisopropylethylamine (DIPEA) (2.30 mL, 13.20 mmol) and chloroform (CHCl₃) (15 mL) were added to the reaction mixture and refluxed overnight. Then, DCM (30 mL) was added and the solution was extracted with water (30 mL). The aqueous layer was extracted twice with DCM (30 mL). The organic fractions were combined and dried with Na₂SO₄, filtered and the solvent was removed on a rotary evaporator before purification by column chromatography (PE/EtOAc 100/0-0/100 v/v). The product was concentrated by rotary evaporation and dried in vacuum to obtain an oil. Yield: 63%, 1.77 g. ^{1}H-NMR (CDCl₃, 400 MHz): 7.44-7.41 (d, 6H), 7.21-7.15 (t, 6H), 7.11-7.05 (t, 3H), 5.12 (br s, 1H), 4.15-4.12 (m, 2H), 3.61-3.55 (m, 12H), 3.48-3.45 (m, 2H), 3.29 (s, 3H), 3.10-3.03 (m, 2H), 2.08-2.04 (t, 2H), 1.41-1.37 (m, 4H), 1.25-1.14 (12H, m). ^{13}C-NMR (CDCl₃, 100 MHz): 156.23, 146.12, 128.3, 127.46, 125.87, 71.68, 70.60, 70.34, 70.31, 70.24, 69.40, 68.64, 66.78, 63.46, 60.03, 54.41, 43.30, 40.75, 30.61, 29.72, 29.35, 29.28, 29.05, 27.10, 26.51. MALDI-TOF-MS: m/z calcd: 648.41; found: 671.74 [M+Na]$^+$.

Compound 8B. Compound **6** (0.78 g, 3.55 mmol) was activated with CDI (0.64 g, 3.95 mmol) for 1h at room temperature. Subsequently, compound **7** (1.61 g, 3.88 mmol), DIPEA (2.00 mL, 5.74 mmol) and CHCl₃ (15 mL) were added to the reaction mixture and refluxed overnight. Then, DCM (30 mL) was added and the solution was extracted with water (30 mL). The aqueous layer was extracted twice with DCM (30 mL). The organic fractions were combined and dried with Na₂SO₄, filtered and the solvent was removed in rotary evaporator before purification by column chromatography (PE/EtOAc 100/0-0/100 v/v). The product was concentrated by rotary evaporation and dried in vacuum to obtain an oil. Yield: 74 %, 1.74 g. ^{1}H-NMR (CDCl₃, 400 MHz): 7.52-7.48 (d, 6H), 7.31-7.25 (t, 6H), 7.21-7.17 (t, 3H), 4.87-4.83 (br s, 1H), 4.32-4.20 (t, 2H), 3.72-3.68 (m, 12H), 3.41-3.38 (m, 2H), 3.20-3.13 (m, 2H), 2.15-2.11 (t, 2H), 1.51-1.44 (m, 4H), 1.35-1.26 (m,

12H). ^{13}C-NMR (CDCl$_3$, 100 MHz): 146.46, 128.76, 127.82, 126.23, 70.97, 70.81, 70.78, 70.76, 70.63, 70.16, 69.80, 69.06, 66.93, 63.91, 50.78, 43.67, 41.15, 30.97, 30.05, 29.71, 29.62, 29.38, 27.45, 26.85. MALDI-TOF-MS: m/z calcd: 659.40; found: 659.12 [M+H]$^+$.

Compound 9A. Compound **8A** (1.68 g, 2.58 mmol) was dissolved in TFA (1 mL) stirred at room temperature for ~ 20 min. When the reaction was complete (as determined by TLC), the TFA was removed by a gentle stream of air and the solid was redissolved in CHCl$_3$ (15 mL). Subsequently, 3,4-dibutoxy-3-cyclobutene-1,2-dione (0.68 mL, 3.13 mmol) and DIPEA (6.00 mL, 34.44 mmol) were added to the reaction mixture and refluxed overnight. Then, DCM (30 mL) was added and the solution was extracted with water (30 mL). The aqueous layer was extracted with DCM (2 x 30 mL). The organic fractions were combined and dried with Na$_2$SO$_4$, filtered and the solvent was removed in rotary evaporator prior to purification by column chromatography (PE/EtOAc 100/0-0/100 v/v). The product was then concentrated by rotary evaporation and dried in vacuum to obtain an oil. Yield: 87%, 1.26 g. ^{1}H-NMR (CDCl$_3$, 400 MHz): 7.14 (s, 1H), 4.96 (s, 1H), 4.71-4.62 (m, 2H), 4.16-4.13 (t, 2H), 3.63-3.56 (m, 12H), 3.52-3.48 (m, 2H), 3.40-3.32 (m, 5H), 3.12-3.05 (m, 2H), 1.78-1.68 (m, 2H), 1.58-1.51 (m, 2H), 1.44-1.41 (m, 4H), 1.26-1.18 (m, 12H), 0.94-0.89 (t, 3H). ^{13}C-NMR (CDCl$_3$, 100 MHz): 189.75, 182.75, 177.46, 172.51, 156.54, 73.41, 71.96, 70.62, 70.57, 70.55, 70.53, 69.69, 63.85, 60.46, 44.93, 41.06, 32.08, 30.69, 29.96, 29.73, 29.42, 29.23, 29.13, 26.73, 26.40, 18.71, 13.73. MALDI-TOF-MS: m/z calcd: 558.35; found: 580.86 [M+Na]$^+$.

Compound 9B. Compound **8B** (1.74 g, 2.64 mmol) was dissolved in TFA (1 mL) stirred at room temperature for ~ 20 min . When the reaction was complete (as determined by TLC), the TFA was removed by a gentle stream of air and the product was redissolved in CHCl$_3$ (15 mL). Subsequently, 3,4-dibutoxy-3-cyclobutene-1,2-dione (0.68 mL, 3.13 mmol) and DIPEA (5.00 mL, 28.70 mmol) were added to the reaction mixture and refluxed overnight. Then, DCM (30 mL) was added and the solution was extracted with water (30 mL). The aqueous layer was extracted twice with DCM (30 mL). The organic

fractions were combined and dried with Na_2SO_4, filtered and the solvent was removed in a rotary evaporator prior to purification by column chromatography (PE/EtOAc 100/0-0/100 v/v). The product was concentrated by rotary evaporation and dried in vacuum to obtain an oil. Yield: 47%, 0.71 g. ^{1}H-NMR (CDCl$_3$, 400 MHz): 7.00-6.95 (m, 1H), 4.87-4.84 (m, 1H), 4.72-4.64 (m, 2H), 4.20-4.16 (t, 2H), 3.70-3.62 (m, 12H), 3.41-3.34 (m, 4H), 3.14-3.09 (m, 2H), 1.79-1.71 (m, 2H), 1.61-1.56 (m, 2H), 1.46-1.37 (m, 4H), 1.31-1.24 (m, 12H), 0.95-0.92 (t, 3H). ^{13}C-NMR (CDCl$_3$, 100 MHz): 189.79, 182.83, 177.62, 172.99, 172.51, 156.54, 73.49, 70.79, 70.75, 70.72, 70.61, 70.15, 69.76, 68.97, 67.15, 63.93, 50.78, 44.99, 41.11, 32.11, 31.13, 30.73, 29.99, 29.45, 29.26, 29.16, 26.76, 26.43, 18.75, 13.78. MALDI-TOF-MS: m/z calcd: 569.34; found: 591.40 [M+Na]$^+$.
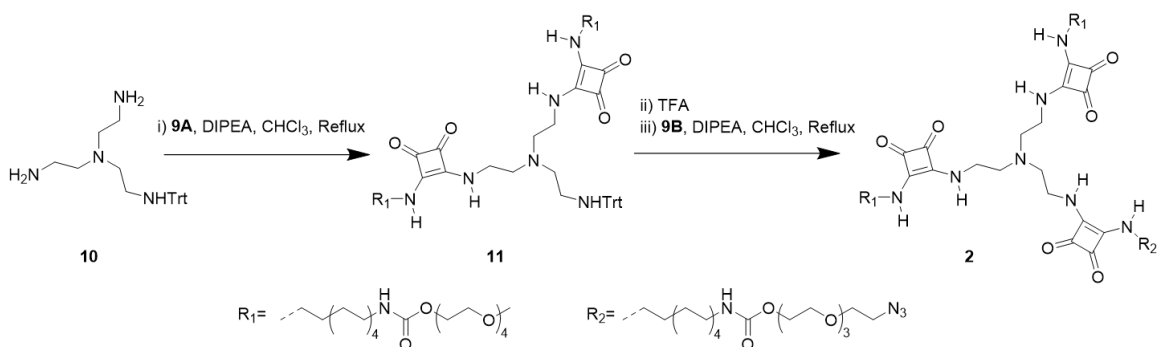
Scheme S2.3. Synthetic route for compound **3**.

Compound 10. Tris(2-aminoethyl)amine (2.99 g, 20.47 mmol) was dissolved in dry DCM (100 mL) and triphenylchloromethane (1.02 g, 3.66 mmol) in dry DCM (100 mL) was added dropwise at room temperature. The mixture was stirred overnight and then washed with 10 wt% NaOH solution (100 mL) and brine (100 mL). The organic phase was dried over Na_2SO_4 and concentrated in rotary evaporator. The crude was purified by column chromatography (DCM/MeOH/NH$_4$OH 100/0/0-85/15/0.1 v/v/v). The product was concentrated by rotary evaporation and dried in vacuum to give compound **10** as a yellowish oil. Yield: 62%, 0.88 g. ^{1}H-NMR (CDCl$_3$, 400 MHz): 7.51-7.48 (d, 6H), 7.31-7.26 (t, 6H), 7.21-7.16 (t, 3H), 2.69-2.65 (t, 4H), 2.62-2.58 (t, 2H), 2.36-2.32

(t, 4H), 2.26-2.22 (t, 2H). ^{13}C-NMR (CDCl$_3$, 100 MHz): 146.26, 128.68, 127.91, 126.36, 70.77, 57.51, 55.06. 41.04, 39.83. HR-MS: [M+H]$^+$: calcd: 389.2700, found: 389.2696.

Compound 11. Compound **9A** (0.52 g, 0.93 mmol) was dissolved in CHCl$_3$ (10 mL) in a round bottom flask. Compound **10** (0.16 g, 0.41 mmol) and DIPEA (0.50 mL, 2.87 mmol) were added before refluxing the reaction mixture overnight. The crude was concentrated and purified by column chromatography (EtOAc/MeOH 100/0-100/20 v/v). The product was concentrated by rotary evaporation and dried in a vacuum oven to obtain an oil. Yield: 54%, 0.30 g. ^{1}H-NMR (CDCl$_3$, 400 MHz): 8.23 (br s, 2H), 8.05 (br s, 2H), 7.41-7.38 (d, 6H), 7.22-7.17 (t, 6H), 7.13-7.08 (t, 3H), 5.08 (br s, 2H), 4.20-4.17 (t, 4H), 3.66-3.51 (m, 32H), 3.35 (s, 6H), 3.17-3.07 (m, 4H), 2.60-2.55 (m, 8H), 1.61-1.54 (m, 4H), 1.46-1.39 (8H, m), 1.27-1.22 (m, 24H). ^{13}C-NMR (CDCl$_3$, 100 MHz): 182.73, 181.77, 168.95, 167.16, 156.66, 128.75, 127.91, 126.36, 71.96, 70.57, 70.54, 70.50, 69.88, 63.86, 55.87, 54.42, 44.80, 42.67, 41.21, 31.15, 30.07, 29.83, 29.64, 29.61, 29.41, 29.39, 26.91, 26.68. MALDI-TOF-MS: m/z calcd: 1356.82; found: 1379.95 [M+Na]$^+$.

Compound 3. Compound **11** (0.15 g, 0.11 mmol) was dissolved in TFA (1 mL) and stirred at room temperature for ~ 20 min. When the reaction was complete (as determined by TLC), the TFA removed by a gentle stream of air and the solid was redissolved in CHCl$_3$ (15 mL). Subsequently, compound **9B** (0.08 g, 0.14 mmol) and DIPEA (3.00 mL, 17.22 mmol) were added to the reaction mixture and refluxed overnight. The crude was concentrated and purified by column chromatography (EtOAc/DCM/MeOH 100/0/0-0/100/0-0/100/10 v/v/v). The product was concentrated by rotary evaporation and dried in vacuum oven to obtain a sticky solid. Yield: 56%, 0.10 g. ^{1}H-NMR (CDCl$_3$, 400 MHz): 7.90-7.80 (m, 6H), 5.12-5.00 (m, 3H), 4.20-4.18 (t, 6H), 3.71-3.53 (m, 52H), 3.39-3.36 (m, 6H), 3.14-3.09 (q, 6H), 2.78 (br s, 6H), 1.61-1.24 (m, 50H). ^{13}C-NMR (CDCl$_3$, 100 MHz): 182.92, 169.48, 167.09, 156.69, 72.03, 70.86, 70.82, 70.80, 70.66, 70.62, 70.59, 70.22, 69.90, 69.86, 63.94, 59.21, 50.78, 44.99, 41.24,

31.27, 30.14, 29.72, 29.50, 26.98, 26.74. LC-MS: t = 6.84 min, m/z: 1610.52. MALDI-TOF-MS: m/z calcd: 1609.98; found: 1631.48 $[M+Na]^+$.
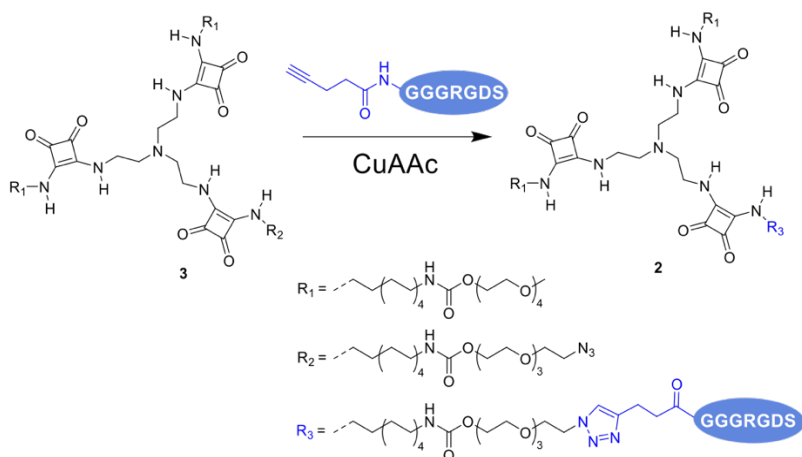
Scheme S2.4. Synthesis of compound **2**.

Peptide synthesis. RGD Peptides (GGGRGDS, **PEP1**) were synthesized on an automatic CEM peptide synthesizer on a 100 µmol scale. Fmoc-Rink amide AM resin with a loading capacity of 0.74 mmol/g was used. Amino acid coupling was performed with 4 eq. of the amino acid, 4 eq. of the activator HCTU and 8 eq. of DIPEA. Fmoc-deprotection was executed using pyridine: dimethylformamide (DMF) (2:8 v/v). The peptides were cleaved in a TFA solution with 2.5% H_2O and 2.5% Triisopropylsilane (TIPS) for 2h, precipitated in cold diethyl ether, dried and dissolved in water prior to injection into LCMS. **PEP1**: LC-MS: t =0.69 min, m/z calcd: 604.26, found: 604.47$[M+H]^+$.

Coupling of the alkyne functionality. Coupling of the alkyne was manually performed on the solid phase. Briefly, the obtained resins (100 µmol) from the peptide synthesizer were suspended in DMF (2 mL) for 15 min. 4-Pentynoic acid (53.3 mg, 0.54 mmol) was coupled to the N-terminus of the peptide by incubation with HCTU (206.8 mg, 0.50 mmol) and DIPEA (175 µL, 1.00 mmol) in DMF (4 mL) at room temperature for 1h. Afterwards, the alkyne-functionalized peptides were cleaved from the resin using a TFA solution with 2.5% H_2O and 2.5% TIPS for 2h and precipitated in cold diethyl ether,

70

dissolved in water, and lyophilized to obtain a pale-yellow solid. The alkyne-functionalized RGD peptides were presented as **PEP2**. The products were confirmed by LC-MS. **PEP2**: LC-MS: t =0.69 min, m/z calcd:684.28; found: 684.40 [M+H]$^+$.

Compound 2. Sodium L-ascorbate (38.0 mg, 191.9 µmol) and copper (II) sulfate pentahydrate (6.4 mg, 25.6 µmol) were first dissolved separately in water (100 µL) and then, mixed using a vortex for 30s resulting in a bright yellow solution. Afterwards, tris(3-hydroxypropyltriazolylmethyl) amine (THPTA, 5.5 mg, 12.6 µmol) dissolved in ethanol (200 µL) and compound **2** (51.6 mg, 32.0 µmol) dissolved in DMF (1.2 mL) were added to the mixture. Lastly, **PEP2** (43.8 mg, 64.0 µmol) dissolved in DMF:H$_2$O (400 µL, v/v 1:1) was added and the reaction mixture was stirred at room temperature for 2h. The crude was first dialyzed against water (Mw 500-1000 Da) for 48 h and purified by HPLC. The product was concentrated by evaporation and lyophilized overnight to obtain a white solid. Yield: 35%, 34.9 mg. LC-MS: t = 5.86 min, m/z calcd: 2295.27; found: 1148.27 [M+1] /2.

2.6.4 Two-component squaramide-based supramolecular hydrogel preparation method

Compound **1** was synthesized and prepared as a hydrogel as previously reported. [3] However, to prepare the two-component hydrogels with peptide-labelled monomers, a three-step protocol was used. First, stock solutions of compound **1** (25 mM in DMSO) and compound **2** (5 mM in DMSO) were made separately, and then pipetted with the appropriate ratios into a new vial and vortexed to obtain a transparent mixture. The mixed solutions in DMSO were left overnight under a gentle flow of nitrogen to yield a dry film. The films were suspended in PBS (pH 7.4) at a final monomer concentration at 3.44 mM in a sterilized flow cabinet, followed by 30 s vortex and sonication in ice-water bath until transparent solutions were obtained (~30 min). Lastly, the transparent

solutions were incubated at 37°C for 30 min and left on the bench overnight at room temperature prior to further testing.
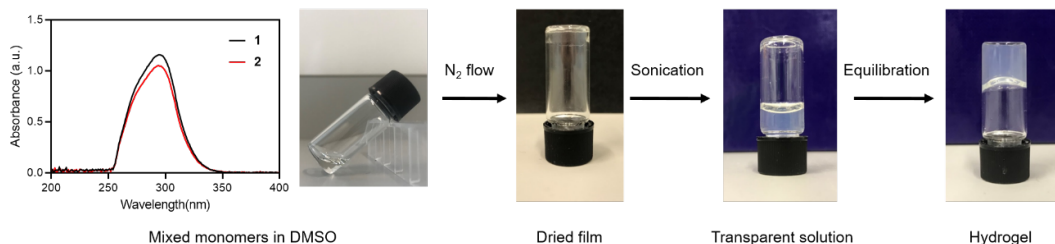
Figure S2.1. Workflow for the preparation of RGD-functionalized squaramide hydrogels. 1) UV spectra show that the squaramide monomers are depolymerized in DMSO due to a broad band centered around 293 nm. 2) Preparation of a mixture of monomer **1** and **2** starting from their respective DMSO stock solutions. 3) Representative image of a film obtained after applying a gentle flow of nitrogen gas overnight. 4) Dried films in PBS (pH 7.4) were sonicated for ~30 min in an ice-water bath (4 °C) until transparent solutions were obtained. 5) Transparent hydrogels are formed after incubation of the vial at 37°C for 30 min and being left to stand at room temperature overnight.

2.6.5 Oscillatory rheology

The mechanical properties of the squaramide-based hydrogels were measured on a Discovery HR-2 hybrid rheometer using cone-plate geometry (40 mm, 1.995°) at 37 ± 0.2 °C with a Peltier-based temperature controller and a solvent trap. Hydrogels with various molar percentages of monomer **2** (SQ-2RGD, SQ-5RGD, SQ-10RGD, SQ-15RGD) were prepared according to the protocol above to result in a total final monomer concentration of 3.1 mM. The hydrogels (600 μL) were left to stand overnight and then pipetted onto the lower plate and the geometry was lowered to a gap distance of 54 μm. Time sweep measurements were executed at a frequency of 1.0 Hz and strain of 0.05% and frequency sweeps were conducted from 0.01–2 Hz with 0.05% strain. Subsequently, a step-strain measurement was performed after a plateau in the storage

modulus was reached in the time sweep. Then, 100% strain was applied to the squaramide-based hydrogels for 120 s. The hydrogels were left to recover for 20 min while measuring at 0.05% strain (f = 1.0 Hz), during which the storage modulus returned to the original plateau. The measurement was repeated for two cycles. Lastly, an amplitude sweep was performed within the strain range from 0.01% to 100% to determine the linear viscoelastic regime (f = 1.0 Hz).
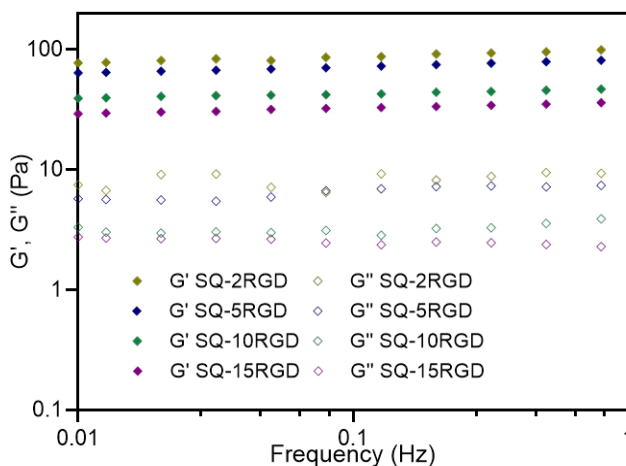
Figure S2.2. Frequency sweep measurements of RGD-functionalized squaramide hydrogels in PBS (pH 7.4) at 37 ± 0.2 °C. Frequency sweep data was collected in a range of 0.01 Hz to 2 Hz with strain of 0.05%. (N = 3)
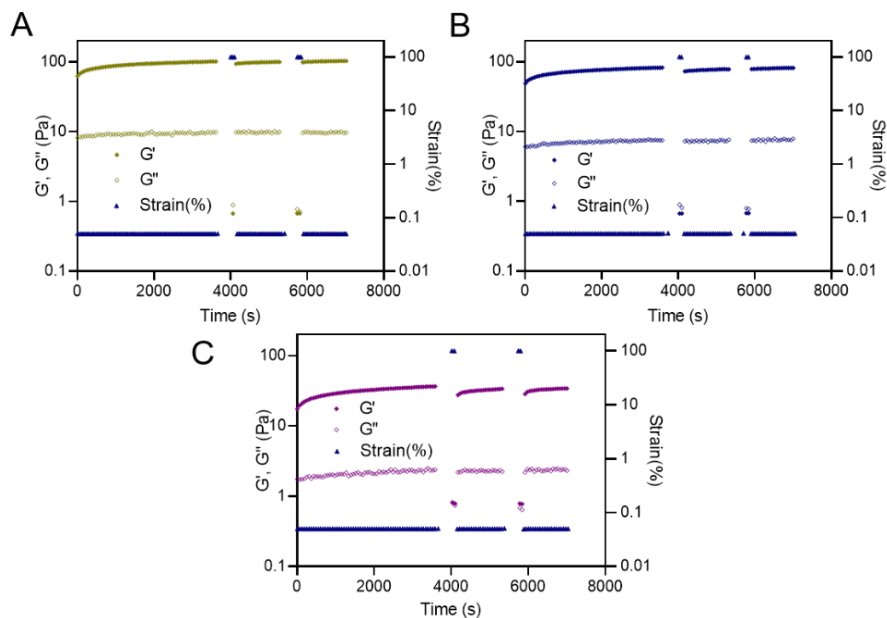
Figure S2.3. Step-strain measurement of RGD-functionalized squaramide hydrogels in PBS (pH 7.4) at 37 ± 0.2 °C. The data were collected at a frequency of 1 Hz. The absence of data between the application of low and high strain is due to the acquisition of a frequency sweep (from 0.01 to 2 Hz, γ= 0.05%) in between these steps. (N = 3)
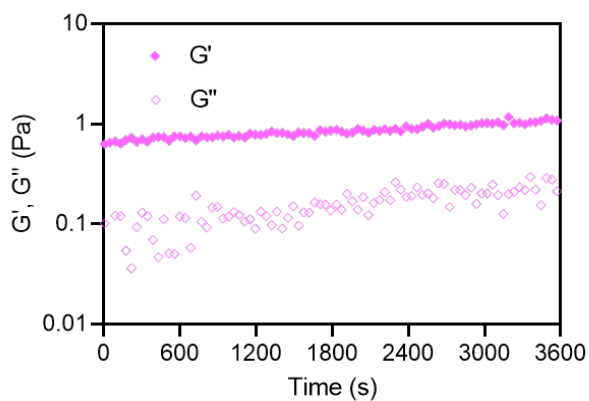
Figure S2.4. Time sweep measurement of SQ-40RGD solution at 37 ± 0.2 °C. Time sweep measurements with strain at 0.05% and frequency of 1 Hz.

2.6.6 Cryo-TEM

Cryo-TEM images of the vitrified samples were acquired with a Tecnai F12 (FEI Company, The Netherlands) equipped with a field emission gun operating at 120 keV using a Gatan UltraScan charge-couple device (CCD) camera (Gatan company, Germany) with a defocus between −6 and −9 μm. Cryo-TEM samples were prepared by applying 3 μL of a SQ-10RGD, hydrogel (3.1 mM) and a SQ-40RGD solution (3.1 mM) to a freshly glow-discharged 300 mesh copper grid with a lacey-carbon support film (Supplier-Electron Microscopy Sciences, Pennsylvania, USA). Excess liquid was blotted away for 2 s (95% humidity, 21 °C, Whatman No. 4 filter paper) and plunge-frozen in liquid ethane at −196 °C using a Leica EM GP (Leica Microsystems, Wetzlar, Germany). The samples were stored in liquid nitrogen before imaging.
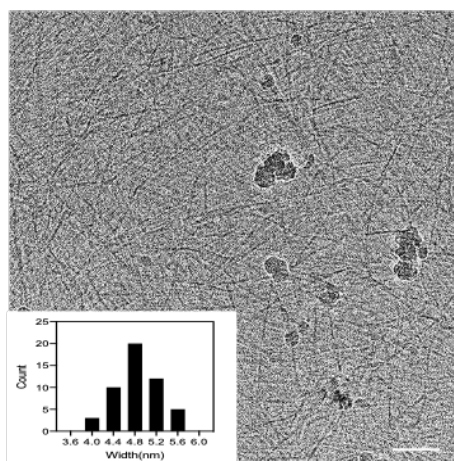
Figure S2.5. Cryo-TEM image of SQ-10RGD hydrogel (3.1 mM, PBS, pH 7.4) as prepared by the gelation protocol. Scale bar: 100 nm. Insert image: histograms of fibre width distribution collected from a sample size N = 50.
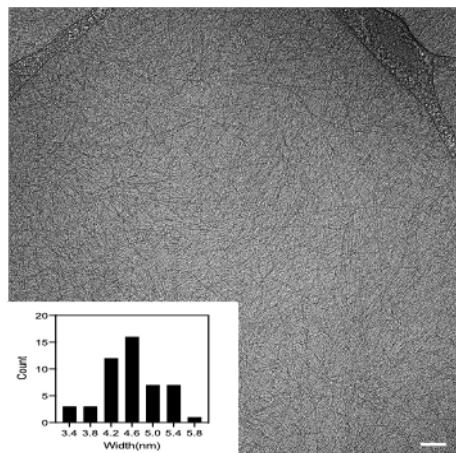
Figure S2.6. Cryo-TEM image of SQ-40RGD solution (B) (3.1 mM, PBS, pH 7.4) as prepared by the gelation protocol above. Scale bar: 100 nm. Insert image: histograms of fibre width distribution collected from a sample size N = 50.

2.6.7 UV−Vis Spectroscopy

UV-Vis spectra were recorded on a Cary 300 UV-Vis spectrophotometer using a quartz cuvette with a path length of 1 cm. The dry film of monomers mixture was prepared according to gelation protocol above. Then, the films were suspended in PBS (pH 7.4) at a final monomer concentration of 1.0 mM, followed by vortexing for 30 s and sonication (~20 min) in ice-water bath to obtain transparent solutions. The solutions were left to stand overnight and diluted into 30 μM with PBS (pH 7.4) prior to measurement.
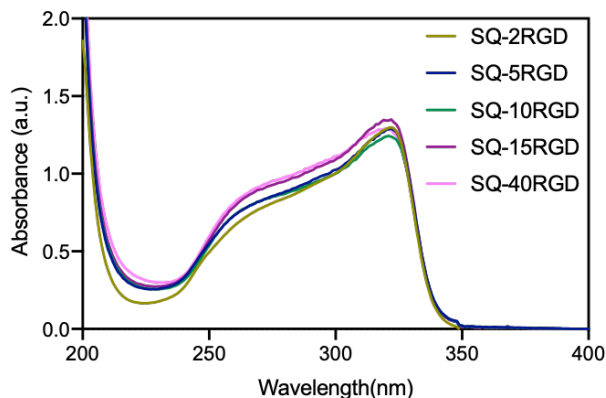
Figure S2.7. UV-Vis spectra of squaramide-based supramolecular polymer solutions (30 µM) containing 2-40 mol% **3** in PBS (pH7.4).

2.6.8 NIH 3T3-LifeAct- mCherry cell migration and spreading in 3D

NIH 3T3 fibroblasts with mCherry-LifeAct were cultured in high glucose DMEM supplemented with 10% newborn calf serum (NCS), 1% Glutamax, and 0.2% penicillin-streptomycin in a 37 °C incubator with 5% CO_2. The cells were kindly provided by T. Schmidt (LION, Leiden University) and previously transduced with LifeAct-mCherry through lentiviral infection. [4] In culture, cells were selected for expression of LifeAct-mCherry with 2 µg/ml puromycin. The culture was maintained with a confluency below 70%. Prior to seeding into hydrogel, NIH3T3-LifeAct-mCherry cells cultured in T-75 flask were dissociated and re-suspended in DMEM medium with a final cell concentration at $2.5×10^7$ cells/mL. The cell suspension (50 µL) and the prepared hydrogel (450 µL) were mixed by gentle pipetting and transferred to the µ-Slide 8 well (200 µL/well). After gelation at 37 °C for 15 min, the hydrogels were mounted with fresh medium for cell culture. Five positions per well were chosen and time-lapse confocal imaging was performed over 20 hours. Images were captured every 5 minutes under a 40x air objective (Nikon) on a Nikon Eclipse Ti microscope equipped with a confocal spinning disk unit operated at 10,000 rpm (Yokogawa). Images were captured using an exposure time of 300 ms by an Andor iXon Ultra 897 High Speed EM-CCD camera (Andor

Technology). During imaging, cells were kept at 37 °C and 5% CO_2 in a humidity-controlled incubator (Tokai hit). To quantify cell-gel interaction by cell spreading efficiency, cells were cultured under various conditions (SQ, SQ-5RGD, SQ-10RGD, SQ-15RGD) for 24-hours and then imaged. Cell-laden hydrogels were prepared as described above, but with a final cell density at 1×10^6 cell/mL to ensure single cell resolution during edge-detection. After preparation, the cell-gel mixture was pipetted into custom-made mini-well inserts, 20 mm x 30 mm (~20 µL/well), placed in larger 4-well µ-Slides (Ibidi). The well inserts were fabricated as previously described. [5] After gelation, at 37 °C for 15 min, each mini-well was submersed in 1 mL high glucose DMEM medium. After 24-hours, a volume-slice (1.2 mm x 1.2 mm x 0.15 mm, 2.5 µm z-stacks) of each gel was imaged under the same objective, starting at a height of least 50 µm into the gel (above the bottom of the slide). The mCherry fluorescent protein was excited using a 0.2W 561 nm solid-state diode laser (Coherent) supported in an Agilent MLC4 unit (Agilent Technologies), at reduced intensity and controlled by an Acousto-Optic Tunable Filter. Images were captured using an exposure time of 500 ms by an Andor iXon Ultra 897 High Speed EM-CCD camera (Andor Technology). An in-house Matlab (Mathworks) code was used to quantify cell spreading, which allows automated adaption of edge-detection settings for every individual cell recognized. Before edge detection, all images were flattened using FIJI plugin BaSiC [6] and then imported into Matlab. The cell-edge is defined as the perimeter of pixels at the boundary of the cell area in the binary mask. Using the binary mask, the cell area, perimeter, summated skeleton branch length and Feret-diameters were calculated using the scale (0.3449 µm/pix). The skeleton of each cell was found by reducing the area to a line using their corresponding binary image (*bwskel* algorithm, MATLAB 2019a). Circularity and Aspect Ratio were calculated based on following equations.

$$Circularity = (4 * pi * Area)/(Perimeter^2)$$

equation 1

$$Aspect\ Ratio = Min\ Feret\ Diameter/Max\ Feret\ Diameter$$

equation 2
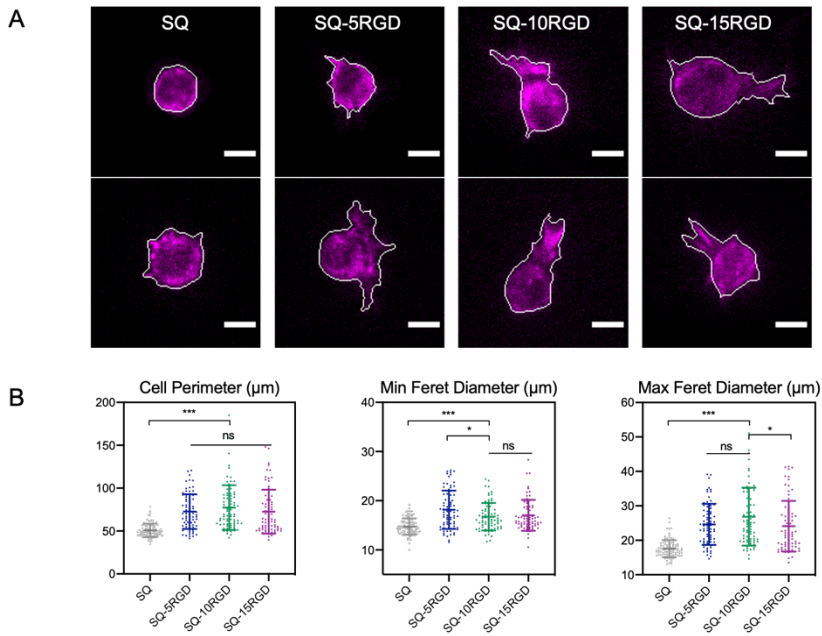
Figure S2.8. A) Representative images of NIH3T3-LifeAct-mCherry cultured within squaramide-based hydrogels, scale bar: 10 µm; B) Quantitative analysis of cell perimeter, minimum and maximum Feret diameter of NIH3T3-LifeAct-mCherry cells cultured for 24h within squaramide-based hydrogel in 3D. The means and standard deviations are marked inside the graphs.

Table S2.1. Summary of quantitative analyses (mean ± 95% confidence intervals)

	SQ	SQ-5RGD	SQ-10RGD	SQ-15RGD
Number of cells	100	76	78	74
Area (μm^2)	183.0±7.3	296.3±23.1	266.5±19.0	261.6±18.6
Perimeter (μm)	50.8±1.3	72.7±3.9	77.3±4.9	72.6±5.0
Circularity	0.903±0.022	0.726±0.030	0.619±0.038	0.694±0.042
Skeleton branch length (μm)	5.2±1.2	20.3±3.3	22.4±3.3	20.00±3.6
Min Feret diameter (μm)	14.7±0.2	18.2±0.8	16.7±0.5	17.0±0.6
Max Feret diameter (μm)	17.6±0.4	24.6±1.1	26.9±1.59	24.1±1.4
Aspect ratio	0.844±0.01	0.750±0.02	0.662±0.028	0.741±0.026

2.6.9 HepG2 cell encapsulation and culture in 3D

HepG2 cells cultured in a T-75 flask were first trypsinized, counted and re-suspended in DMEM/F12 supplemented with 10% (v/v) fetal bovine serum (FBS), 25 U/mL penicillin

and 25 µg streptomycin and diluted to a final cell concentration of 1×10^6 cells/mL. The cell suspension (20 µL) and the pre-prepared squaramide-based hydrogel (180 µL) according to the gelation protocol were mixed through by gentle pipetting and then, the cell-gel suspension–was ~~were~~ transferred to an angiogenesis slide (12 µL/well). After being left to stand at 37 °C for 15 min, the hydrogels were mounted with an additional amount of medium (48 µL) for cell culture. For Growth Factor Reduced Matrigel (Corning) encapsulation, Matrigel was diluted to 5 mg/mL and cells were cultured as previously described.[7] The medium was refreshed twice per week during the three-week culture period in the same volume.

2.6.10 Spheroids diameter determination

HepG2 spheroids were imaged using the EVOS FL AUTO2 equipped with a temperature and CO_2 gas controller at pre-defined time points. Z-stack images were acquired under a 10× objective and an environment of 37°C and 5% CO_2 was maintained during the measurement. The spheroid diameter was measured in Fiji by drawing a straight line horizontally (angle < 3°) with the corresponding scale. Sixty-six spheroids were counted for each group.

2.6.11 LIVE/DEAD staining

At pre-determined time points, the medium on top of the hydrogel was removed by pipetting, rinsed twice with PBS (pH 7.4, 45 µL) and incubated with a prepared staining solution (48 µL) (calcein AM (2 µM) and propidium iodide (1.5 µM)) at 37 °C for 30 min. The staining solution was removed and the hydrogel was rinsed again with PBS two times (48 µL). The stained cell-laden hydrogel was imaged with Leica TCS SP8 confocal laser scanning microscope equipped with a 10× air objective. Fluorescent images were acquired at a resolution of 1024 × 1024 pixels using an excitation wavelength of 488

nm and an emission filter of 500–545 nm for calcein AM and an excitation wavelength of 532 nm and an emission filter of 594–686 nm for propidium iodide.
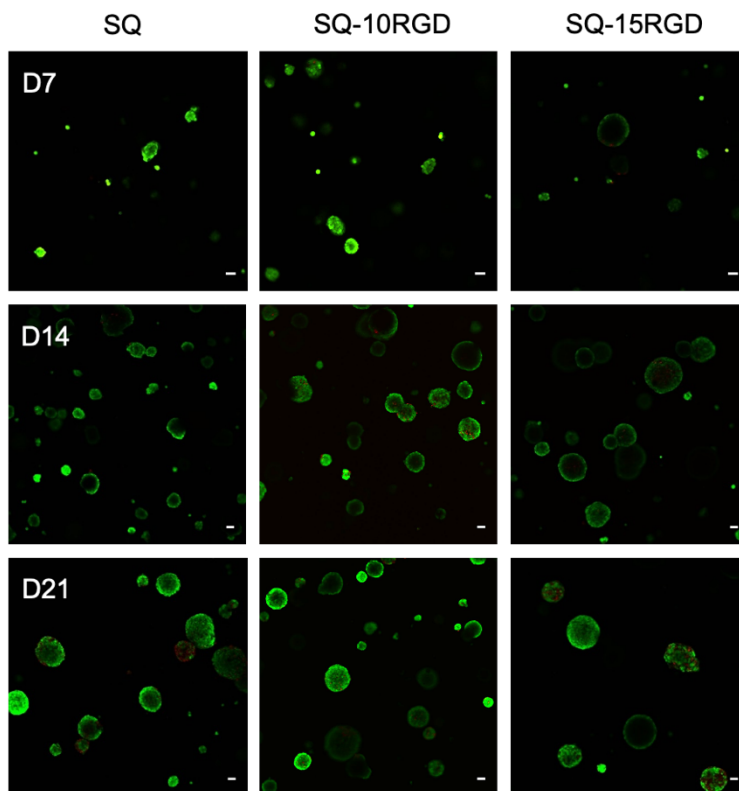
Figure S2.9. Cell viability assay of HepG2 spheroids over the a 21-day culture period. LIVE/DEAD staining with calcein AM (viable cells, *green*) and propidium iodide (PI) (dead cells, *red*). Scale bar: 50 μm.

2.6.12 EdU staining

At pre-determined time points, cell-laden hydrogels were first diluted with cold medium (4 °C) (100x volume), pipetted and spun down to collect the HepG2 spheroids. Proliferating cells were labelled according to the protocol described in the Click-iT EdU Alexa Fluor 594 Imaging Kit. Briefly, the released HepG2 spheroids were first treated with the EdU solution (10 μM) at 37°C for 4h. Afterwards, the cells were fixed with 5% (w/v) PFA solution for 15 min at room temperature, followed by a 20-min penetration

by 0.5% (w/v) Triton X-100 at room temperature. After washing with BSA solution (3%), the cells were incubated with the Click-iT® reaction cocktail for 30 min, followed by another wash and hoechst 33342 (5 µg/mL) incubation for 30 min to stain cell nuclei. The stained cell sample was transferred into another chamber slide that is protected from light and imaged on Leica TCS SP8 confocal laser scanning microscope equipped with a 40× oil immersion objective. Fluorescent Z-stack images were acquired at a resolution of 1024 × 1024 pixels with a step size at 1 µm. The Z-stack images from 3D HepG2 spheroids were projected into 2D by Fiji. Corrected total cell fluorescence (CTCF) for both channels were measured by Fiji and EdU positive ratios were calculated based on according to following equation:

$$CTCF = Integrated\ Density - (area\ of\ selected\ cell \times$$
$$Mean\ fluorescence\ of\ background\ reading)$$

equation 3

$$EdU\ positive\ ratios = CTCF_{EdU}/CTCF_{Hoechst} \times 100\%$$

equation 4

In each measurement, three random areas around the cell were measured as background. Three spheroids were measured for all the groups.
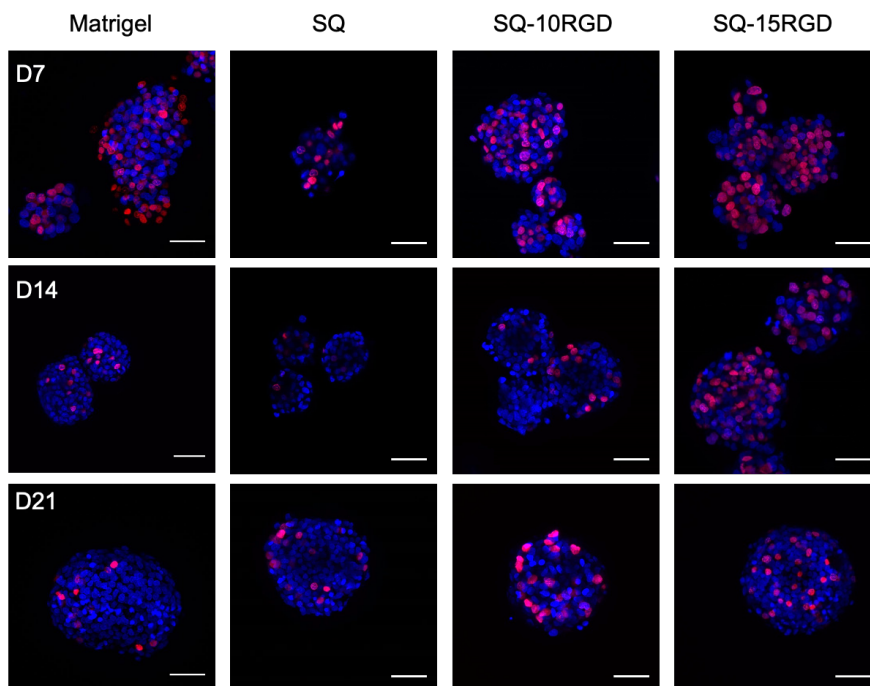
Figure S2.10. Representative images of EdU staining in HepG2 spheroids released during culture in Matrigel and squaramide-based hydrogels. Proliferating cells were labelled with EdU-Alexa fluor 594 (*red*) and cell nuclei were stained with Hoechst 33342 (*blue*). Scale bar: 50 μm.

2.6.13 RT-PCR

The cell-laden hydrogels were cultured at 37°C as previously described. On day 21, the total RNA was extracted using the TRI Reagent. RNA yield and purity were determined using the NANODROP spectrophotometer. 800 ng RNA was used to generate cDNA construct using the RevertAid H Minus First Strand cDNA Synthesis Kit. For RT-qPCR, 5x diluted cDNA was mixed with 1 μM forward and reverse primers (Table S2) and X10 POWRUP SYBR MASTER MIX. Parameters used for RT-qPCR were: 50 ºC for 2 minutes, 95 ºC for 10 minutes, followed by 40 cycles at 95 ºC for 15 seconds and 60 ºC for 1 minute, 95 ºC for 15 seconds, 60 ºC for 1 minute, and finally 95 ºC for 15 seconds and run on a QuantStudio™ 6 Flex Real-Time PCR System (Applied Biosystems®). Samples

were measured in triplicate and mRNA expression was quantified using the delta-delta Ct (2–ΔΔCt) method. GAPDH was used as housekeeping gene.

Table S2.2. Primer sequences

Gene	Forward 5'- 3'	Reverse 5' -3'
CYP3A4	TTCCTCCCTGAAAGATTCAGC	GTTGAAGAAGTCCTCCTAAGCT
CYP1A2	CTTTGACAAGAACAGTGTCCG	AGTGTCCAGCTCCTTCTGGAT
CYP3A5	CTCTCTGTTTCCAAAAGATACC	TGAAGATTATTGACTGGGCTG
CYP2D6	CCTACGCTTCCAAAAGGCTTT	AGAGAACAGGTCAGCCACCACT
CYP2C9	GAACACCAAGAATCGATGGACA	TCAGCAGGAGAAGGAGAGCATA
CYP2C19	CAACAACCCTCGGGACTTTA	GTCTCTGTCCCAGCTCCAAG
AAT1	ACTGGGGTGACCTTGGTTAAT	GACGGCATTGTCGATTCACTG
UGT1A1	CAGCAGAGGGGACATGAAAT	ACGCTGCAGGAAAGAATCAT
HNF4a	ACTACGGTGCCTCGAGCTGT	GGCACTGGTTCCTCTTGTCT
MRP2	GGCAGTGAAGAAGAAGACGATGA	ATTGGACCTAGAACTGCGGCT
NCTP	ATCGTCCTCAAATCCAAACG	CCACATTGATGGCAGAGAGA
Albumin	ATGCTGAGGCAAAGGATGTC	AGCAGCAGCACGACAGAGTA
GAPDH	CTGGTAAAGTGGATATTGTTGCCAT	TGGAATCATATTGGAACATGTAAACC
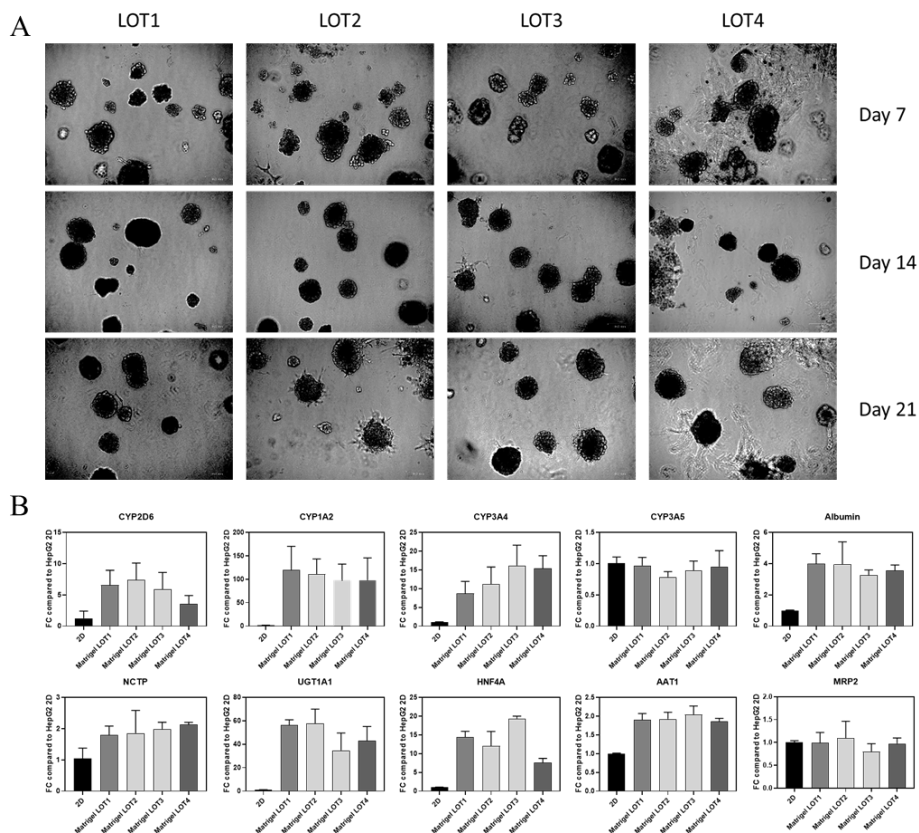
Figure S2.11. A) 3D HepG2 cell culture in four different LOTs of Matrigel (LOT5215008, LOT2326787, LOT5061003 and LOT2104930): A) Bright field images taken on day 7, 14 and 21. B) Fold change hepatic gene expression levels of HepG2 spheroids after a 21-day culture in Matrigel in comparison to 2D on tissue culture plates. (N = 3)

2.6.14 Immunofluorescence Analysis

Cells were cultured at 37℃ as previously described. On day 21, the spheroids were fixed with 4% PFA for 30 minutes. Subsequently, the samples were blocked and permeabilized in 0.2% Triton X-100, 0.5% BSA in 1X PBS (TBP) for 1 hour. Spheroids were stained with the primary antibodies against albumin (1:1000, Bethyl laboratories, A80-229F), MRP2 (1:50, Abcam, M2III6) and β-catenin (1:50, Invitrogen, 71-7200) in TBP overnight at 4℃. After washing the samples three times in 1X PBS, spheroids were

counter-stained with secondary antibodies (1:1000, Molecular probes, A11001, A11008), Hoechst 33342 (2µg/mL, Sigma) and Rhodamine Phalloidin (1:10.000, Sigma, P1951) in TBP for 1 hour at room temperature and finally washed three times with 1X PBS. Images were acquired with a Nikon TiE2000 confocal microscope with a 20X objective and 2X zoom.
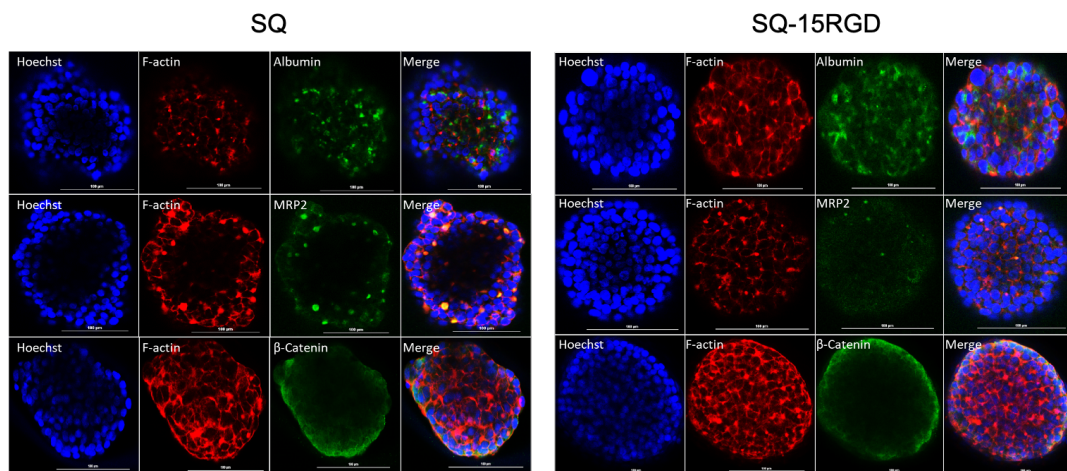
Figure S2.12. Immunofluorescence staining of the liver markers albumin (upper row), MRP2 (middle row) and β-catenin (lower row) in green counter-stained with F-actin rhodamine phalloidin (*red*) and the nuclear staining Hoechst33342 (*blue*). Merged channels consist of all three stains. Scale bar: 100 µm

2.6.15 References

[1]   K. D. Park, R. Liu, H. Kohn, *Chem. Biol.* **2009**, *16*, 763.

[2]   A. M. Albrecht-Gary, S. Blanc, F. Biaso, F. Thomas, P. Baret, G. Gellon, J. L. Pierre, G. Serratrice, *Eur. J. Inorg. Chem.* **2003**, 2596.

[3]   C. Tong, T. Liu, V. Saez Talens, W. E. M. Noteborn, T. H. Sharp, M. M. R. M. Hendrix, I. K. Voets, C. L. Mummery, V. V. Orlova, R. E. Kieltyka, *Biomacromolecules.* **2018**, *19*, 1091.

[4]   H. van Hoorn, Cellular Forces : Adhering, Shaping, Sensing and Dividing, Dr.Thesis, Leiden University, **2014**.

[5]   C. Tong, J. A. J. Wondergem, D. Heinrich, R. E. Kieltyka, *ACS Macro Lett.* **2020**, *9*, 882.

[6]   T. Peng, K. Thorn, T. Schroeder, L. Wang, F. J. Theis, C. Marr, N. Navab, *Nat. Commun.* **2017**, *8*, 1.

[7]   S. C. Ramaiahgari, M. W. Den Braver, B. Herpers, V. Terpstra, J. N. M. Commandeur, B. Van De Water, L. S. Price, *Arch. Toxicol.* **2014**, *88*, 1083.